Journal Pre-proof

Morphological and Mechanical Variations in E. coli Induced by PMMA Nanostructures Patterned via Electron Beam Lithography: an Atomic Force Microscopy Study

Paolo Pellegrino , Isabella Farella , Valeria De Matteis , Mariafrancesca Cascione , Matteo Calcagnile , Stefania Villani , Lorenzo Vincenti , Pietro Alifano , Fabio Quaranta , Rosaria Rinaldi

PII: S2468-0230(24)01862-5
DOI: https://doi.org/10.1016/j.surfin.2024.105707
Reference: SURFIN 105707

To appear in: *Surfaces and Interfaces*

Received date: 1 October 2024
Revised date: 6 December 2024
Accepted date: 23 December 2024

Please cite this article as: Paolo Pellegrino , Isabella Farella , Valeria De Matteis , Mariafrancesca Cascione , Matteo Calcagnile , Stefania Villani , Lorenzo Vincenti , Pietro Alifano , Fabio Quaranta , Rosaria Rinaldi , Morphological and Mechanical Variations in E. coli Induced by PMMA Nanostructures Patterned via Electron Beam Lithography: an Atomic Force Microscopy Study, *Surfaces and Interfaces* (2024), doi: https://doi.org/10.1016/j.surfin.2024.105707

This is a PDF file of an article that has undergone enhancements after acceptance, such as the addition of a cover page and metadata, and formatting for readability, but it is not yet the definitive version of record. This version will undergo additional copyediting, typesetting and review before it is published in its final form, but we are providing this version to give early visibility of the article. Please note that, during the production process, errors may be discovered which could affect the content, and all legal disclaimers that apply to the journal pertain.

© 2024 Published by Elsevier B.V.

Journal Pre-proof

Morphological and Mechanical Variations in *E. coli* Induced by PMMA Nanostructures Patterned via Electron Beam Lithography: an Atomic Force Microscopy Study

Paolo Pellegrino[1,2], Isabella Farella[1*], Valeria De Matteis[1,2], Mariafrancesca Cascione [1,2]*, Matteo Calcagnile[3], Stefania Villani[4], Lorenzo Vincenti[2], Pietro Alifano[3], Fabio Quaranta[1] and Rosaria Rinaldi [1,2]

[1]Institute for Microelectronics and Microsystems (IMM), CNR, Via Monteroni, 73100 Lecce, Italy
[2]Department of Mathematics and Physics "E. De Giorgi", University of Salento, Via Monteroni, 73100 Lecce, Italy
[3]Department of Experimental Medicine, University of Salento, Via Monteroni, 73100 Lecce, Italy
[4]Department of Engineering for Innovation (DII), Campus Ecotekne, University of Salento, Via Monteroni, 73100 Lecce, Italy

Journal Pre-proof

Abstract

Nanostructured antibacterial surfaces have recently gained significant interest for their ability to mechanically disrupt bacterial cells and reduce populations. This study presents an efficient method for fabricating PMMA nanostructures using Electron Beam Lithography, focusing on nanograting and nanopillar arrays with pitches ranging from 160 to 200 nm. Atomic Force Microscopy was employed to characterize these structures. The antibacterial efficacy was assessed against *Escherichia coli* revealing a significant reduction in bacterial adhesion, grown on the nanostructures compared to the flat PMMA surfaces, with the nanopillars showing a more pronounced effect (about 85%) compared to the nanogratings (75%). The bacteria exhibited significant shape changes and damage, indicative of severe cellular disruption. Detailed AFM analysis confirmed notable morphological changes, including reduced major axis length, decreased surface area, and increased roughness, probably due to membrane

rupture. Nanomechanical studies on the cell surface revealed changes in *E. coli* Young's modulus and adhesion forces, further demonstrating that nanostructures play a role. The Young's modulus of *E.coli* changes from (1.5 ± 0.2) MPa on flat PMMA (control) to (0.7 ± 0.1) MPa on nanograting with a pitch of 160 nm (lower pitch) and (0.5 ± 0.1) MPa on nanopillars with a pitch of 200 nm (higher pitch). Similarly, the adhesion forces of bacteria grown on flat PMMA were (1.8 ± 0.1) nN while they increased to (7.2 ± 0.1) nN and (14.8 ± 1.4) nN for lower-pitch nanogratings and higher-pitch nanopillars, respectively. These findings highlight the potential of nanostructured surfaces as advanced antibacterial materials.

1. Introduction

Microbial infections, stemming from the colonization of pathogenic microorganisms in susceptible hosts, pose a significant challenge to the scientific community, representing a global threat to public health and resulting in substantial economic burdens. [1]. To counter the omnipresence of these microorganisms, intensive efforts have been dedicated to devising robust methodologies to fight against their proliferation. The discovery of penicillin by Alexander Fleming in 1928 and subsequent antibiotics in the 20th century revolutionized the treatment of bacterial infections [2] [3]. These antibiotics were highly effective at killing bacteria and exhibited minimal toxicity to host cells, making them the primary therapeutic approach for bacterial infections well into the 21st century [4], [5] [6]. However, due to an excessive and indiscriminate use of antibiotics, multi-drug resistant (MDR) bacteria have emerged.

The increasing prevalence of antibiotic-resistant microorganisms has emerged as a significant global crisis, comparable to climate change and pandemic outbreaks [6]. The misuse and suboptimal utilization of antibiotics, particularly in economically disadvantaged regions

such as the Asia-Pacific, Africa, and South America, exacerbate this issue [6][7]. Consequently, major pharmaceutical companies have shifted their focus from antibiotic research toward established therapeutic areas like oncology, diabetology, and cardiovascular medicine [8]. Annually, antibiotic-resistant infections result in over 700,000 deaths, with projections indicating this could escalate to 10 million by 2050 if left unchecked [9]. The financial burden is equally substantial, with treatment costs averaging US$50,000 per case and societal costs reaching US$20 billion annually [10]. These alarming figures highlight the urgent need for mandatory interventions.

In 2021, the World Health Organization (WHO) released a comprehensive list of antibiotic-resistant pathogens, highlighting those deemed priority pathogens. This list notably emphasized the threat posed by resistant Gram-negative bacteria, such as *Pseudomonas aeruginosa*, *Acinetobacter baumannii*, and *Enterobacteriaceae*, which represent a hazardous risk to human health [11]. The rising prevalence of MDR bacteria imposes a drastic breakthrough in their management and several strategies are currently being explored, as those offered by nanotechnologies. An approach has been the development of several types of nanomaterials, *i.e.* metal nanoparticles (gold, silver, iron oxide, and zinc oxide) [12] [13] [14] [15], carbon-based nanomaterials [16] [17] [18], liposomes [19] [20], biopolymers [21] [22] [23], nanoemulsion and smart nanomaterials [24], [25], [26]. A more interesting strategy in preventing or reducing bacterial adhesion and biofilm formation, and even in killing microorganisms upon contact, is the exploitation of nanostructured surfaces. Drawing inspiration from natural structures found on animal bodies, including cicada and dragonfly wings [27] [28] [29] [30], shark skin [31], [32], and gecko feet [33] [34], as well as plant surfaces like lotus leaf [35], and replicating them onto surfaces of relevant objects (surgical or medical implantable devices), it becomes feasible to strategically exploit those characteristics

Journal Pre-proof

selected by evolution over time, empowering our defensive capabilities against pathogenic bacteria with additional arms.

Different nano- and microscale topographies, including nanoridges, ripples, and grooves, have been successfully fabricated using both top-down and bottom-up approaches. Notably, nanopillar arrays exhibit some of the most effective antibacterial activities [36] [37]. Previous studies suggest that the bactericidal effect of the nanopillars arrays, inspired by cicada and dragonfly wings, is due to the physical stretching of microbial cells upon contact, resulting in the lysis and subsequent death of bacteria[37] [38] [39] [40] [41]. Besides the rupture and lysis of bacteria, nanostructured surfaces have also been found to modify the genomic and proteomic profiles of bacteria [42]. The effectiveness of these substrates has been proven for various Gram-negative and Gram-positive bacteria, such as *P. aeruginosa* [43] [37] [44] [45], *Pseudomonas fluorescens* [28], *Klebsiella pneumoniae* [42] [46], *Staphylococcus aureus* [41] [42] [47] [38], *Staphylococcus epidermidis* [48] *Escherichia coli* [42] [43], [47], [49], and *Bacillus subtilis* [38] [46].

Despite the well-documented bactericidal effects of both natural and synthetic nanopillars [9], the underlying mechanism of microbial cell death remains unclear, highlighting the complexity of this phenomenon. Although several mechanisms have been proposed, the experimental and analytical constraints make it challenging to ascertain the precise contributions and interactions among these mechanisms. In particular, there is ongoing debate regarding the contribution of factors such as surface water contact angle, surface roughness, and nanostructure spacing to the bactericidal efficacy of nanostructured surfaces [50], [51]. Furthermore, while numerous antibacterial nanostructures with similarities to those in this study have been reported, a comprehensive direct comparison is challenging due to significant differences in composition and geometry. These include variations in size, height, dimensions, and surface randomness, as outlined in reference [41].

In this context, the present study investigates the interaction of Gram-negative *E. coli* bacteria with nanostructured Poly(methyl methacrylate) (PMMA) surfaces, specifically nanogratings and nanopillar arrays patterned by Electron Beam Lithography (EBL), a powerful top-down nanofabrication method for the realization of nanostructures on PMMA [52] [53]. Given the frequent association of *E. coli* with infections on medical implants, such as prostheses and urinary catheters, it is of paramount importance to gain insight into its response to nanostructured surfaces.

The primary objectives of this research are twofold: firstly, to develop a simple yet effective electron beam lithography (EBL)-based method for fabricating precise nanograting and nanopillar arrays in a positive-tone resist, such as PMMA [54] [55], and secondly, to examine the morphological and mechanical responses of *E. coli* to these nanostructures. By employing this methodology, high-accuracy nanostructured substrates with lateral periods between 160 and 200 nm were successfully fabricated. Following the fabrication of the substrate, a combination of Atomic Force Microscopy (AFM) and Ultra High-Resolution Scanning Electron Microscopy (UHR SEM) was employed to conduct a detailed examination of the bacterial adherence to the nanopatterned surfaces, with a particular focus on changes in bacterial cell morphology. The analysis encompassed a range of parameters, including surface roughness, elongation, surface area coverage, and cell volume. Additionally, a comprehensive cytomechanical analysis was performed to quantify the impact of nanostructures on the surface properties of *E. coli*. These insights collectively contribute to the advancement of two distinct fields: nanofabrication and biomedical device design. They enhance our comprehension of the influence of nanoscale topography on bacterial behavior at the cellular level.

2. Materials and Methods

2.1 Fabrication of nanostructured surfaces

Two types of nanostructured surfaces were fabricated for this study: nanogratings (alternating lines of ridges and grooves) and ordered arrays of nanopillars, each with different periods (or pitches), as described as follows. A standard 3-inch non-oxidized siliconwafer (⟨100⟩, p-type boron-doped, resistivity (1-30) Ω cm, (381±25) μm) (Si-Mat Silicon Materials, Kaufering, Germany) was initially cleaned in pure hot acetone and 2-propanol for 15 min. The wafer was then dried under a nitrogen gas stream for approximately 60 sec. Both acetone (99.5%) and 2-propanol (99.5%) were purchased from Sigma-Aldrich. A thin layer of Polymethyl methacrylate (PMMA) A4 (950 kDa, in solvent anisole, MicroChem, Berlin, Germany) was spun onto the silicon substrate at 4000 rpm for 30 sec with a semiautomatic spinner DELTA 80T (SUSS MicroTec Corp, Garching, Germany). The positive-tone resist was then baked at 180 °C for 90 sec on a hotplate to remove anisole solvent. The wafer coated by PMMA was cleaved to obtain a rectangular wide substrate for electron beam exposure. The silicon wafer was chosen to improve sample conductivity and reduce charging effects during the electron beam exposing process. We chose a 1 nA electron beam current with an area dose of 3.1 mC cm^{-2} delivered by a CRESTEC CABLE 1500C (CRESTEC Corporation, Tokyo 192-0045 Japan) EBL system, operating at 46 kV.

Nanogratings were fabricated by patterning parallel lines onto the PMMA (Fig. 1 a). After development, a series of PMMA parallelepipeds, separated by tranches, with controlled periodicity ranging from 160 to 200 nm, in 10 nm steps was created (Fig. 1 b). The arrays of nanopillars were instead fabricated by writing two layers of orthogonal gratings sequentially (Fig. 1 c) [54]. The patterns were designed with the dedicated CAD software of the systems, CABL-2000; the resist was exposed using the Vector scan writing method. The double exposure experienced by the crossing regions of the two overlapping gratings, along with the proper choice of periodicity sorts the effect of rounding the corners of the unexposed positive resist thus giving rise to circular nanopillars (Fig.1 d) [55]. Each array of nanogratings or

nanopillars covered an area of 300 x 300 μm^2 and differed in periodicity (pitch). All arrays with different periodicities, properly spaced, formed a matrix that was accommodated on a single chip. The nano-patterned structures were then developed in a 1:3 methyl isobutyl ketone:isopropanol (MIBK:IPA) solution for 3 min; rinsed in isopropanol for 1 min, and then gently dried out under nitrogen gas flow. After the resist development, the rectangular substrate was cut and the 1 cm^2 wide square chips were separated. Finally, the PMMA layer thickness was measured on a properly patterned test structure using an Alpha-Step P6 profilometer (KLA-Tencor Corporation, Milpitas, CA, USA) and found about 220 nm. The choice of patterning PMMA relies not only on the nanofabrication technique used (EBL) but also on its properties. Besides being a low-cost polymer, transparent, and light-weight, PMMA shows excellent biocompatibility, is a material approved by the United States Food and Drug Administration (FDA), and is widely used in medicine, dentistry, as an implant material for bone cement, intraocular lenses, synovial joints, and dentures [56].

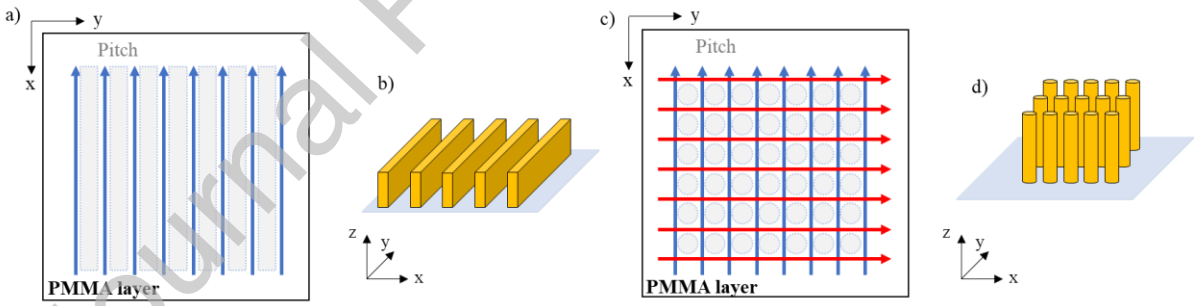

Figure 1: *Scheme of the nanostructures fabrication process and nanopatterns: a) and b) nanogratings; c) and d) nanopillars.*

2.2 Study of the antimicrobial properties against *Escherichia coli*

Journal Pre-proof

E. coli strain FB8 (also known as GC2553, K12S [Luria] or UTH1038, deposited at the University of Texas/Houston stock culture collection, genotype F-l-/lS, ftsR1), is a prototrophic strain [57] [58] [59] and was selected in this study to evaluate the antimicrobial properties of the nanostructured surfaces. *E. coli* was grown in Luria-Bertani (LB) medium, which contained (per liter) 10 g of NaCl, 10 g of Tryptone, 5 g of Yeast Extract, and 15 g of Agar (for LB solid medium). The medium was sterilized by autoclaving at 121 °C for 20 min. *E. coli* pre-inoculum was prepared and incubated with stirring at 37 °C overnight. The following day, the bacterial suspension was adjusted in LB broth to reach an optical density of 0.3-0.4 to obtain the bacterial inoculum for further experimental tests. The PMMA chips were UV-sterilized for 10 min before use. After placing the chips in a 6-well plate (Corning®-Costar® Flat Bottom not treated multiple-well plates) a 200 µl droplet of bacterial inoculum was placed on the top of the samples and then incubated statically at 37 °C for 3 h. Subsequently, the samples were washed twice in 0.9% NaCl solution to remove non-adherent bacteria. To guarantee a uniform distribution of bacteria, the solution was vortexed before pipetting, and a calibrated micropipette was employed to ensure consistent dispensing. Furthermore, gentle agitation of the plate ensured uniform distribution of the bacterial suspension across the surface. Then, samples were fixed with 2.5% glutaraldehyde at 4 °C for 1.5 h and washed three times in ultra-pure distilled water. Finally, the chips were air-dried for 1 h under ambient conditions and stored at 4 °C until further investigations. Bacteria grown on flat PMMA surfaces were used as a control (CTRL).

2.3 AFM studies

The morphology characterization of PMMA nanostructures and *E. coli* cells was performed using an AFM NTEGRA (NT-MDT Spectrum Instruments, Moscow, Russia), operating in semi-contact mode. AFM acquisitions were recorded in Height and SensHeight channels, using NSG01 probes (NT-MDT Spectrum Instruments, Moscow, Russia). These

probes feature a rectangular-shaped cantilever with a typical frequency of 150 kHz and a nominal force constant of 5.1 N/m. The tip is tetrahedral and in the last 500 nm from the tip apex is conical, with a curvature radius of about 6 nm.

NTEGRA AFM was also employed to acquire Force-Distance (FD) curves in contact mode for the nanomechanical characterization of bacteria cells, focusing on elasticity and adhesion forces. Measurements were performed using CSG01 tips (NT-MDT Spectrum Instruments, Moscow, Russia), which feature a cantilever with a resonant frequency of approximately 9.81 kHz and a nominal spring constant of 0.03 N/m. The cantilever has a sharp, tetrahedral-shaped tip at its apex, which has a typical curvature radius of less than 10 nm and a cone angle of less than 20°.

All acquisitions were conducted under ambient conditions (room temperature of about 20 °C and relative humidity of 50 %).

Journal Pre-proof

2.3.1 AFM characterization of PMMA substrates

High-resolution 2D and 3D topographies were obtained for both pristine and patterned PMMA over a scan area of 5 x 5 μm^2 with a resolution of 512 x 512 points. These acquisitions were analyzed to quantify geometrical parameters of the patterned nanostructures, specifically the height, diameter, and pitch of the nanopillars, as well as the period and the height of nanogratings. Before the analysis, each high-resolution AFM image was digitally treated with a second-order plane fit filter and second-order flattening, to suppress three-dimensionality and bow effects.

2.3.2 AFM characterization of *Escherichia coli* surface morphology and Nanomechanics

For *E. coli* cells, acquisitions were recorded over scan areas of 25 x 25 μm^2 and 5 x 5 μm^2 with a resolution of 512 x 512 points. The AFM images were analyzed to measure the

major and minor axes, area, and volume of the cell. In addition, the roughness of the bacterial surface, expressed in terms of root-mean-square surface roughness (R_q) [29], was quantified. The R_q estimation was carried out over fifteen 0.5 x 0.5 μm^2 areas randomly selected on the bacteria surface.

The nanomechanical characterization of the bacteria cells in terms of Young's Modulus (*E*) and the estimation of the adhesion forces were carried out by acquiring 25 FD curves employing the AFM point-and-shoot function on 10 individual cells from three independent experiments. Specifically, the forward data of FD curves were analyzed to quantify the elasticity of bacteria cell surface, expressed in terms of Young's modulus (*E*), using the Sneddon model-based fit:

$$F = \frac{h^2 2E \tan \alpha}{\pi(1-\nu^2)} \qquad (1)$$

where *F* indicates the force applied, *h* corresponds to the displacement of the indenter, *v* is the Poisson's ratio of the sample (taken as 0.5 for biological materials), and α is the half-angle of the conical tip. In equation (1), the *E* is the best-fit parameter, since both *F* and *h* are automatically measured by the AFM.

The backward data of FD curves were analyzed to measure the adhesion forces between the silicon AFM tip and the bacterial surface. These forces were calculated by using Hooke's law:

$$F = k \times \Delta z \qquad (2)$$

where *F* is the adhesion force (nN), *k* is the CSG01 spring constant (N/m) and Δz is the deflection distance (nm), measured between the peak that exhibited the highest adhesion and the baseline zero force level.

Journal Pre-proof

An accurate estimation of the applied force requires quantifying the exact spring constant of the cantilever used to acquire the FD curves; therefore, prior to performing the force spectroscopy study, the spring constant of the CSG01 cantilever was determined using the method of the thermal noise [60].

2.3.3 Scanning Electron Microscopy

Scanning Electron Microscopy (SEM) observations were performed using the TESCAN AMBER FIB-SEM system (TESCAN GROUP, a.s.), equipped with a Ga ion source, Delmic's METEOR system, a Leica VCT500 cryo-transfer unit, and a cryo-stage. SEM imaging was conducted with the samples tilted at an angle of approximately 35°, operating at an accelerating voltage of 1 kV and an AC of 100 pA. To prevent sample charging during imaging, a thin titanium (Ti) layer of about 7 nm was deposited on the samples before SEM characterization.

2.3.4 Software

The NOVA_PX software (NT-MDT Spectrum Instruments, Moscow, Russia) was used to obtain topographic and force-spectroscopy AFM acquisitions.

The Image Analysis P9 (IAP9) software (NT-MDT Spectrum Instruments, Moscow, Russia) was used to analyze all the AFM images and force-spectroscopy analysis, quantify the R_q value, and fit the indentation curves. The modifications in the bacteria cell morphology were quantified by analyzing the high-resolution AFM topographies with the ImageJ 1.53a software. The experimental data were analyzed and plotted using OriginPro, Version 2024b. OriginLab Corporation, Northampton, MA, USA.

2.5 Statistical Analysis

Journal Pre-proof

All the results presented were reported as mean values and associated standard deviation. The difference among data was analyzed through ANOVA multiple comparisons. The differences were statistically significant when * $p < 0.05$.

3. Results and discussion

The PMMA unpatterned substrate further used as a control surface for bacteria inoculation was imaged by AFM. The surface appeared compact and smooth with a roughness R_q value equal to (0.32 ± 0.05) nm.

Following this characterization, the EBL was employed to pattern substrates with nanogratings and nanopillars array. On a single chip, five areas, each 300 x 300 μm^2 in size, were exposed to obtain arrays with different pitches: 160, 170, 180, 190, or 200 nm. The pitch values were used to identify the array fabricated, labeled p160, p170, p180, p190, and p200 to indicate the corresponding distance between adjacent pillars or ridges.

The structural morphology of nanopatterned PMMA was characterized using AFM. The nanogratings (Fig. 2 a-e) exhibited high homogeneity and regularity, with no significant defects or irregularities. Notably, the width of the tranches between two adjacent ridges increased with the pitch.

Journal Pre-proof

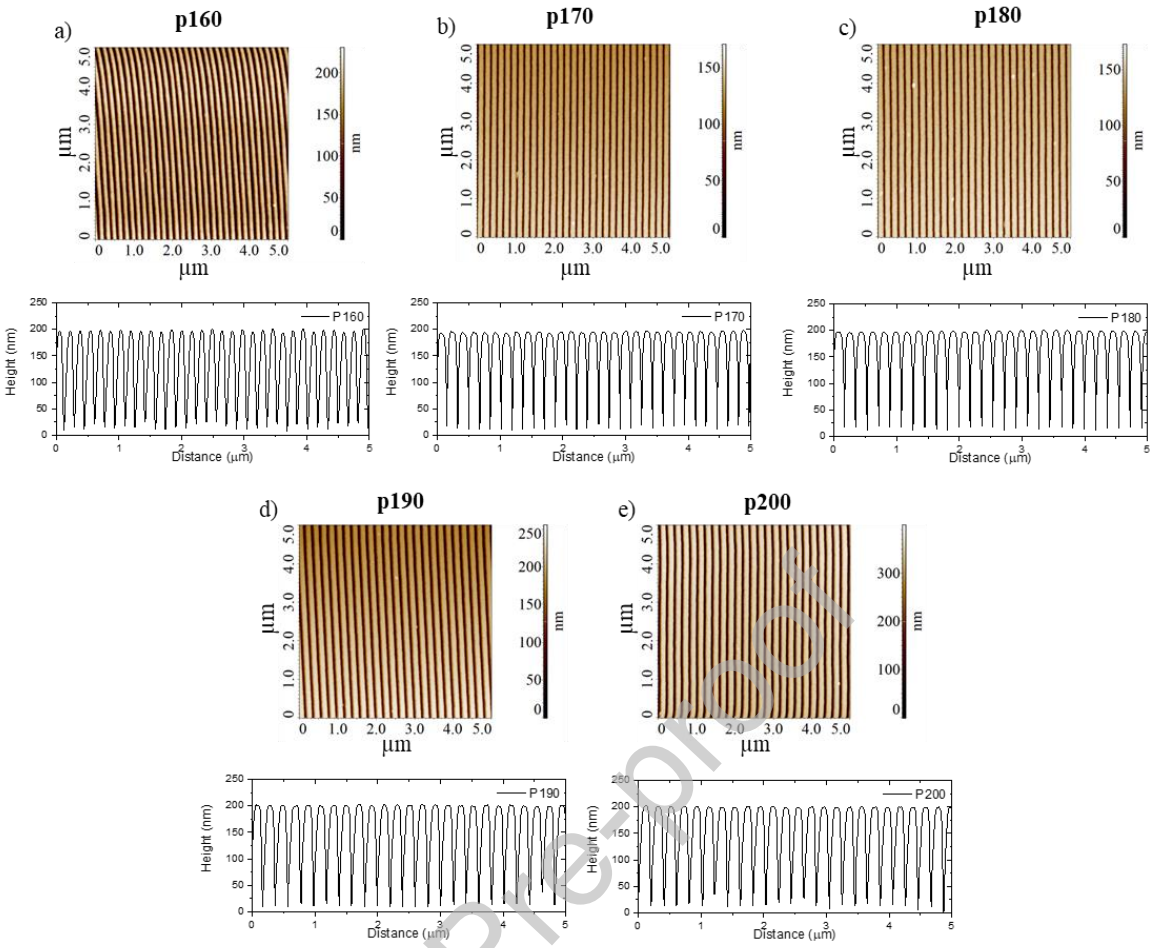

Figure 2*: Two-dimensional high-resolution AFM characterization of nanograting topographies of arrays, and corresponding cross sections randomly selected on each AFM image, with a pitch of a) 160 nm, b) 170 nm, c) 180 nm, d) 190 nm, and e) 200 nm.*

To confirm these observations, the AFM topographies were subsequently analyzed to measure the geometrical characteristics of the nanogratings features, including periodicity (pitch), the ridge height and width, and their corresponding ratio (height to width). The results are reported in ***Table 1***.

Journal Pre-proof

Table1. Geometrical characteristics of PMMA nanogratings

	Pitch ± SD (nm)	Ridge Height ± SD (nm)	Ridge width ± SD (nm)	Aspect ratio
p160	166 ± 6	198 ± 1	108 ± 3	1.83
p170	172 ± 4	197 ± 3	138 ± 5	1.42
p180	182 ± 4	197 ± 3	171 ± 4	1.15
p190	196 ± 4	199 ± 1	190 ± 5	1.05
p200	201 ± 3	207 ± 3	213 ± 4	0.97

The estimated pitch values confirmed the designed periodicity of the nanogratings, corresponding to (166 ± 6) nm, (172 ± 4) nm, (182 ± 4) nm, (196 ± 4) nm, (201 ± 3) nm for the p160, p170, p180, p190, and p200, respectively.

Following a similar procedure, the nanopillar patterns on the PMMA substrate were investigated (Fig. 3 a-e).

Journal Pre-proof

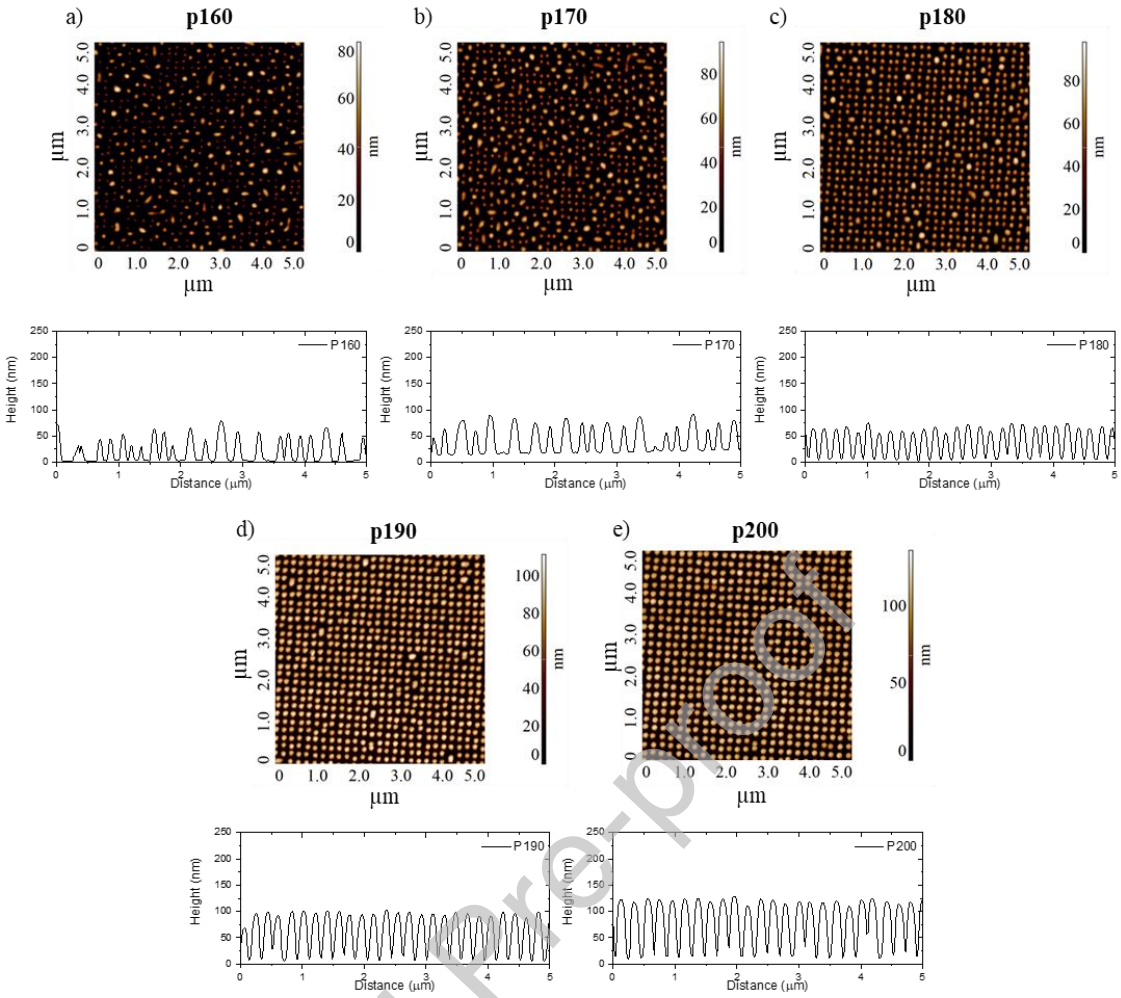

Figure 3: *High-resolution 2D AFM images of nanopillar arrays and corresponding cross sections randomly acquired on each AFM characterization image, with a) 160 nm, b) 170 nm, c) 180 nm, d) 190 nm, and e) 200 nm pitches.*

Journal Pre-proof

At first glance, the order of the nanopillars appeared well-preserved across different pitches. However, p160 and p170 samples exhibited a lower homogeneous distribution of pillar height than samples with a larger pitch. In addition, some pillars appeared taller and wider, suggesting possible attachment or collapse of adjacent nanopillars. This poor homogeneity in height vanishes as the period increases. As the pitches increased arrays are less and less affected by this phenomenon likely caused by proximity effects during EBL exposure.

The 2D high-resolution images were analyzed to measure the dimension of the nanopillars, in terms of the mean pitch, height, diameter, aspect ratio, and density of nanopillars on an area of 5 x 5 μm^2. The results are reported in Table 2.

Table2. Dimensions of the PMMA nanopillars patterned by EBL

	Pitch ± SD (nm)	**Pillars height ± SD (nm)**	**Pillars diameter ± SD (nm)**	**Aspect ratio**
p160	163 ± 33	63.33 ± 33.2	67.7 ± 26.1	1.1
p170	176 ± 23	66 ± 9	73 ± 24	0.90
p180	182 ± 14	73 ± 6	89± 14	0.82
p190	195 ± 14	96 ± 4	91 ± 13	1.06
p200	204 ± 6	121 ± 5	134 ± 10	0.90

Following the AFM analysis, the PMMA nanogratings and nanopillar arrays were further characterized using UHR SEM. As shown in Fig. S1, the SEM images confirm the successful fabrication of the nanostructure arrays, with no significant defects or surface irregularities detected. Consistent with the AFM observations, nanopillar arrays with smaller pitch values (p160 and p170) exhibited less uniform pillar height distribution compared to those with larger pitches (p180, p190, and p200). As reported in high-resolution 2D AFM images (Fig. 3), some nanopillars appeared taller and wider, possibly due to the attachment or collapse of adjacent structures.

The analyzed nanoarrays were used to investigate the effect of both PMMA nanograting and nanopillars on the morpho-mechanical characteristics of Gram-negative bacteria *E. coli*. Before this assessment, the adhesion rates of bacterial cells were evaluated on both the nanograting and nanopillars arrays, as well as on unpatterned PMMA surfaces, which served

Journal Pre-proof

as control. To this aim, 5 topographic AFM images covering an area of 25 x 25 μm^2 were acquired for each sample, and the number of bacteria cells was measured consistently (Fig 4).

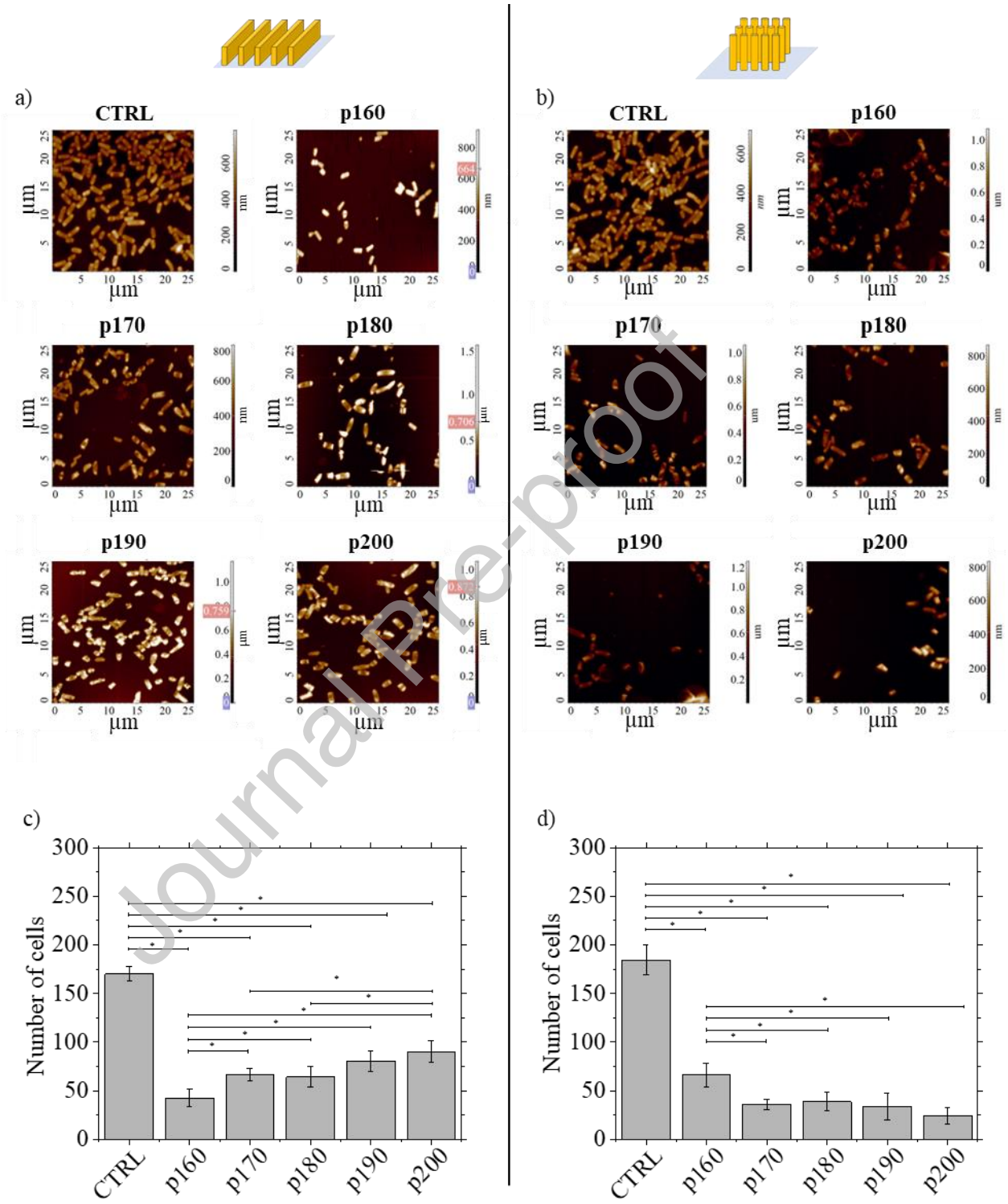

Journal Pre-proof

Journal Pre-proof

Figure. 4. *AFM images of E. coli grown on non-patterned PMMA surfaces, used as a control (CTRL), and on a) nanograting and b) nanopillar arrays with different pitches. Number of bacterial cells on c) nanograting and d) nanopillar array. The data were reported as mean value ± SD. Statistical significance is denoted by * $p < 0.05$.*

Qualitatively, AFM acquisitions revealed a strong reduction in *E. coli* adhesion on both nanostructured PMMA compared to the control (Fig. 4 a, b). Specifically, AFM images indicated a correlation between the *E. coli* adhesion and the pitches of the patterns. For nanograting arrays, an increase in pitch was associated with a slight increase in bacterial count, rising from (43 ± 9) in p160 to (90 ± 11) in the p200 sample (Fig. 4 c). In contrast, for the nanopillar arrays, an increase in pitch led to a significant reduction in the bacterial count, decreasing from (66 ± 12) to (25 ± 8) for the pitch of 160 nm and 200 nm, respectively (Fig. 4 d). This phenomenon can be explained by considering the topographical features of nanogratings with smaller pitches and nanopillars with larger pitches. In particular, the narrower ridge widths (Table 1) and larger nanopillar diameters and heights (Table 2) contribute to this effect. Modifications in these geometric characteristics could modify the interaction processes between bacterial cells and the substrate, potentially impeding *E. coli* adhesion and encouraging bacterial cells to move away from the patterned surfaces. It is conceivable that an increase in nanograting pitch and thus an increase in ridge width provides a wider surface area that facilitates bacterial attachment. Conversely, an increase in nanopillar pitch results in taller and wider nanopillars, which in turn create a more inhospitable environment for bacterial colonization. These results were consistent with other studies reported in the literature [61], [62], [63].

Moreover, the large-scale AFM images acquired on flat PMMA (Fig. 4 a, b), revealed that many *E. coli* cells maintained their typical rod shape with rounded edges. In contrast, cells

on the patterned PMMA surfaces displayed a markedly altered morphology, passing from elongated forms to crumpled and squashed shapes.

To further elucidate the influence of nanostructures on cell morphology, Ultra-High Resolution (UHR) SEM imaging was performed on flat PMMA and nanograting and nanopillar arrays with different pitches (Fig. 5). SEM analysis corroborated preliminary observations from Atomic Force Microscopy images and confirmed distinct morphological changes in *E. coli* as a function of the nanostructure pitch. Specifically, *E. coli* grown on PMMA nanogratings with smaller pitches exhibited pronounced morphological alterations, whereas cells on nanogratings with larger pitches more closely resembled the control morphology (Fig. 5a–f).

In contrast, as the pitch of the nanogratings increased, the bacteria showed a marked transformation, adopting a curled morphology that was significantly different from the control condition (Fig. 5g–l). In addition, UHR SEM analysis revealed evidence of cellular damage, including lysis, particularly on nanopillar arrays with pitches of 180 nm, 190 nm, and 200 nm. This suggests that certain pitch thresholds can induce significant mechanical or structural stress, and consequent rupture, on the bacterial cells (Fig. 5 j–l). Indeed, the bacteria exhibited a deflated morphology as they extended across multiple pillars. The irregular, lumpy appearance of the bacterial *sacculi* on the pillars suggests that the cell membranes were ruptured, resulting in a loss of turgor pressure and, consequently, a loss of the bacterial cytoplasm [56]. All these observations are consistent with the results of the AFM analysis.

Journal Pre-proof

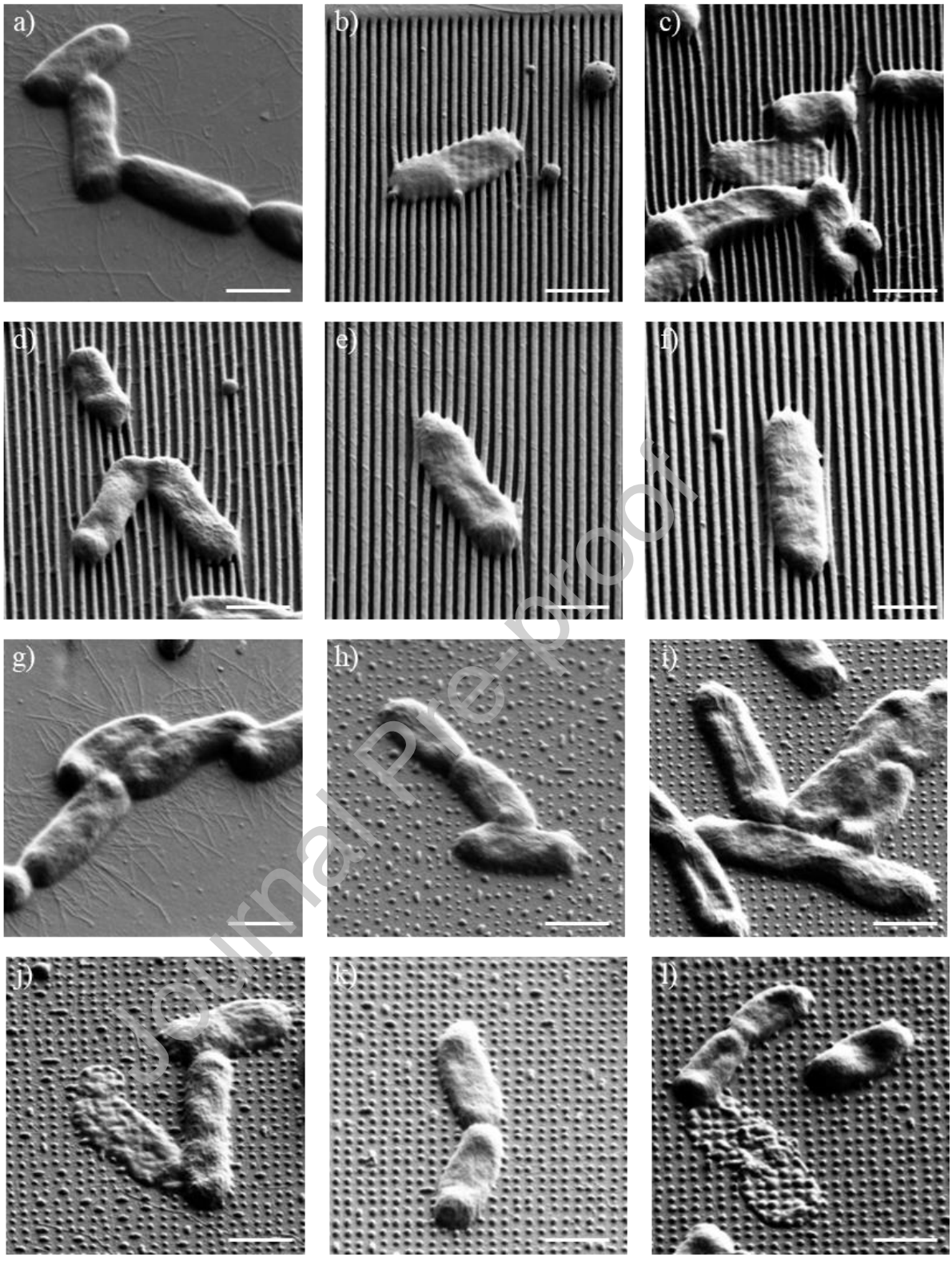

Figure. 5. *UHR SEM images of E. coli grown on a) and g) non-patterned, flat PMMA surfaces (CTRL) and on nanograting with pitches of b) 160 nm, c) 170 nm, d) 180 nm, e) 190 nm, and f) 200 nm. UHR SEM acquisition of E. coli cells on nanopillars array with h) 160 nm, i) 170 nm, j) 180 nm, k) 190 nm, and l) 200 nm pitches, respectively. The scale bars are equal to 1 µm.*

Journal Pre-proof

By analysing both AFM and SEM images, it was possible to quantify the number of damaged *E. coli* cells caused by the interaction with the nanostructures. Specifically, those cells that exhibit a severe modification in their shape, damage on the cell wall, and loss of internal content, are marked as damaged. We assumed the number of damaged cells as an estimation/index of the bactericidal activity of different nanopatterned arrays. In Fig. 6 a), b), c), and d) are reported representative images of damaged cells on nanopatterned PMMA surfaces. The amount of damaged cells, calculated as a percentage of the total *E. coli* population within a 25 x 25 μm^2 area, is reported in Fig 6 e) and f).

Journal Pre-proof

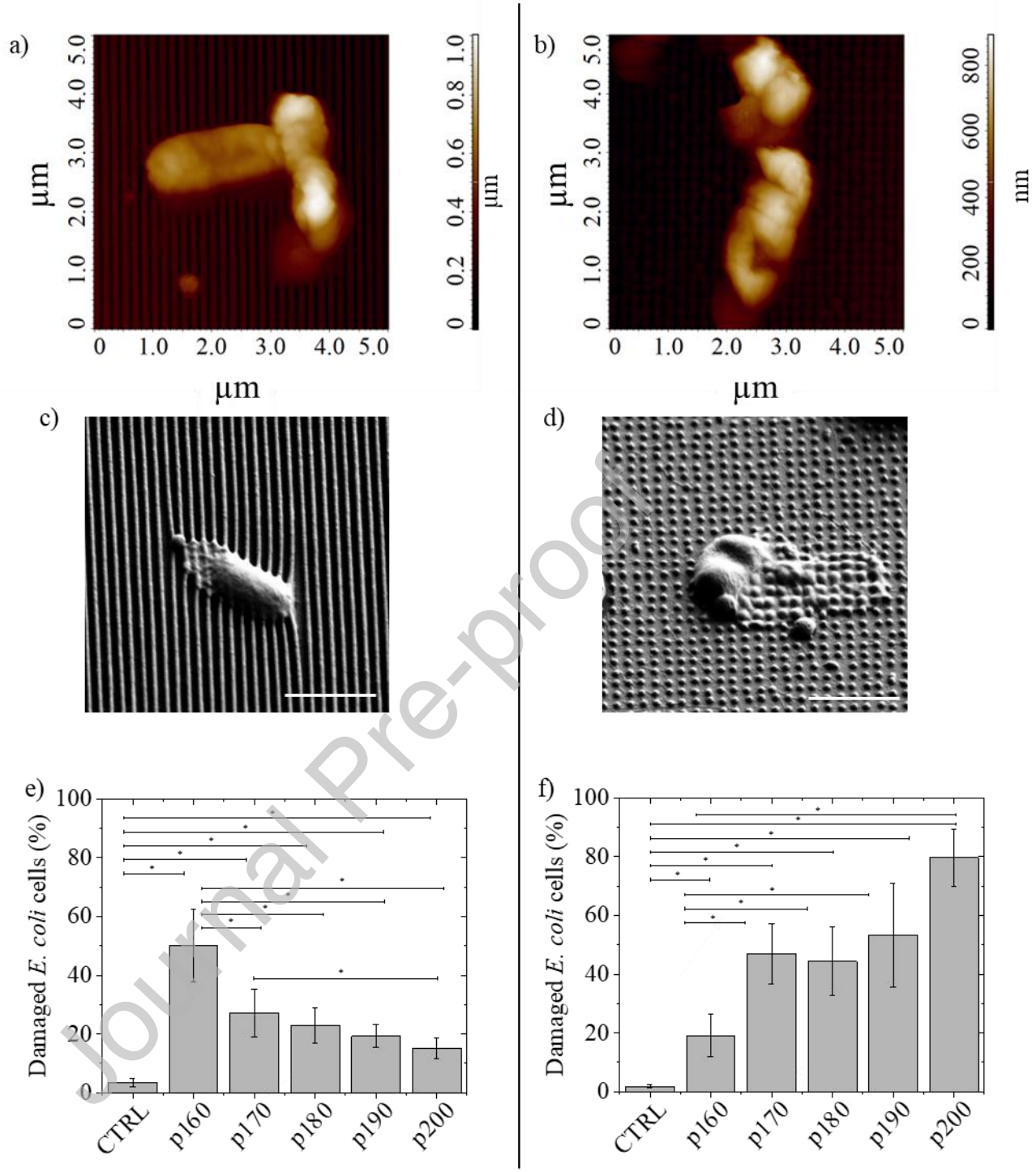

Figure 6: *Representative high-resolution AFM images of damaged E. coli on a) nanogratings with a pitch of 160 nm and b) nanopillars with a pitch of 200 nm and corresponding UHR SEM images c) and d). The scale bars are equal to 1 µm. Estimation of bactericidal activities of various nanostructured surfaces, expressed in terms of the number of bacteria per imaging field whose shape is drastically modified or damaged after interacting with nanogratings e) and nanopillars f) array. The data were reported as mean value ± SD. Statistical significance is denoted by * $p < 0.05$.*

The antibacterial activity against *E. coli* was evaluated for each pitch of PMMA nanograting and nanopillar arrays. Generally, both nanostructures induced significant alterations in the cell wall and drastic modifications in the overall cell morphology. Two distinct trends were observed: as the nanograting pitch increased, the percentage of damaged cells decreased, passing from (50 ± 12) % on the p160 to (15 ± 4) % on p200. Conversely, the percentage of ruptured cells increased with larger nanopillar pitches, rising from (19 ± 7) % on p160 to (80 ± 9) % on p200 arrays. These findings suggest that, as the nanograting interspacing increases, the flat surface area of the ridges becomes larger, providing a more comfortable environment for bacteria adhesion, which in turn may reduce the mechanical stress experienced by the cells. On the other hand, the observed increase in the percentage of damaged *E. coli* on the nanopillar arrays with higher pitches can be attributed to the enhanced geometric characteristics of the nanostructures, such as aspect ratio and diameter (see Table 2). As the density of nanopillars increases, from p160 and p200 samples respectively, the number of contact points between the nanopillars and bacterial cells also increases, potentially enhancing the bactericidal effect. The results show that both the nanopillar and nanograting arrays create a network of nanoprotrusions that increase the surface area of the sample. This increased surface area enhances bacterial adhesion to the nanopillars via strong van der Waals forces, which alone are lethal to bacteria [64] [63]. When bacteria secrete extracellular polymeric substances (EPS) to facilitate attachment and resist environmental, biological and mechanical stresses, an additional layer of EPS is observed [63]. In response, bacteria experience strong shear forces as they attempt to move away from the unfavorable surface (which further explains the reduction in the number of bacteria on the nanopatterned surfaces compared to the flat PMMA, as reported in Figure 4).

During this process, the taller nanopillars lean in the direction of bacterial movement and the nanopillar/nanopatterned layer begins to separate. This strong adhesion, combined with

shear stress, causes deformation of the bacterial membrane. As the immobilized bacterium attempts to move, the stress initiates damage to the bacterial membrane, which is seen as the inner membrane separating from the outer membrane. This membrane rupture leads to cytosol leakage which fills the cavities between the nanostructures, as can also be seen in Figure 6 a), b), c), and d). Eventually, the mechanical integrity of the membrane is severely compromised, causing the bacterial remnants, including the membrane, to collapse onto the nanopillar layer, resulting in bacterial membrane rupture or, in more severe cases, cytoplasm leakage and complete cell lysis [51], [62], [65].

An alternative possible explanation for the observed phenomenon is that nanopatterns could penetrate the bacterial cell wall by puncturing or deforming the entire cell body, causing bacterial death by disrupting the outer cell envelope [56] [51] [9] [66]. The results presented in this paper suggest that the first mechanism is more consistent with our observations.

Morphological variation of E. coli induced by PMMA nanostructure arrays

The variation in the *E. coli* shape was further and accurately investigated by analyzing the high-resolution AFM images, acquired in semi-contact mode over 5 x 5 μm^2 areas (Fig. S2 and Fig. S3). *E. coli* cells grown on flat PMMA exhibited their typical rod-shaped morphology, with no visible damage, rupture, or significant variation in the cell structure (Fig. S2a and Fig. S3a). In contrast, the shape of bacteria on both nanostructures changed dramatically compared to the control. Specifically, bacteria on nanograting with smaller pitches (p160 and p170) (Fig. S2b and Fig.S2c) appeared curled up, while those on the gratings with the larger pitches (p180, p190, and p200) exhibited milder variation in their shape (Fig.S2 d, e, and f). More pronounced alterations in *E. coli* shape were observed in bacteria incubated on the nanopillars arrays. Indeed, as the nanopillars' pitch increased, the bacteria tended to assume a crumpled shape,

resembling a "U"-like folding of their original rod shape (Fig.S3 d, e, and f). To better appreciate this phenomenon, cross-sections of the AFM images of *E. coli* were taken (Fig. 7 a-c).

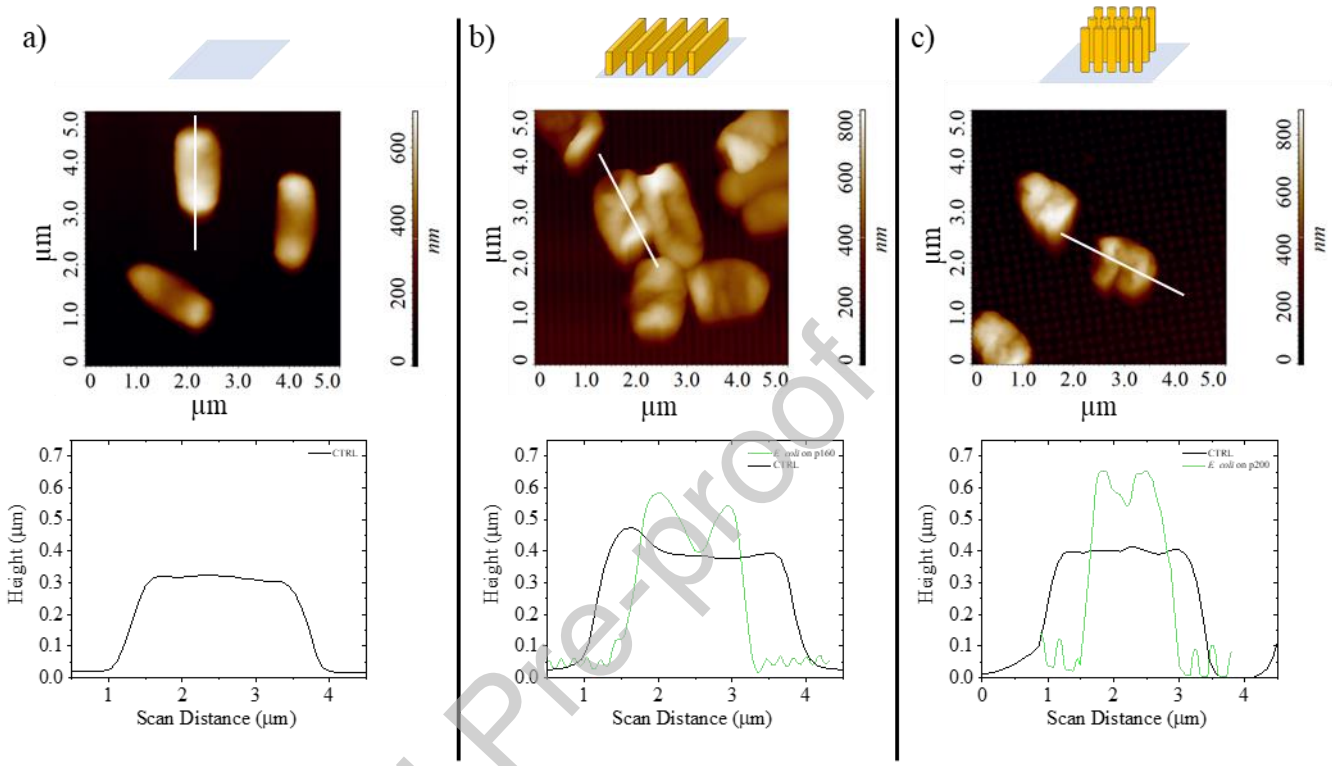

Figure 7. *Representative AFM images of E. coli, on the PMMA sample surfaces (on top), and relative cross sections (white bars) acquired on the cell's major axis, reported on the bottom side of each AFM image. E. coli cell grown on a) flat PMMA, b) nanogratings with pitch 160 nm, and c) nanopillars array with pitch 200 nm. In the graphs, the black curves represent the sections acquired on E. coli cells on flat PMMA (CTRL); the green curves are the sections of bacteria on nanostructures.*

The AFM topographic images were further analyzed to quantify the roughness (R_q) of the *E. coli* surface grown on flat and nanopatterned PMMA (Fig. 8a and b). The R_q surface of bacterial cells on flat PMMA, estimated over 20 different areas of 0.5×0.5 µm^2, was equal to (31 ± 2) nm. This value increased to (68 ± 7) nm for bacteria grown on the p160 nanogratings and it decreased with the increase of the pitch, reaching (39 ± 3) nm on the p200 sample. The

variation in surface roughness of bacteria grown on nanograting arrays is less pronounced than that observed on nanopillars-patterned samples. Notably, in the latter case, an inverse trend was observed: as the distance between the pillars increased, the R_q of the bacterial surface also increased, reaching a maximum of (96 ± 6) nm for the p200 nanopillar samples. This suggests that the change in R_q is mainly influenced by the shape of the nanostructures on which the bacteria grow, which induces changes in the morphology of the bacterial membrane. This phenomenon may be attributed to the mechanical stress exerted by the nanostructured surfaces, leading to membrane disruption and, ultimately, resulting in cell death.

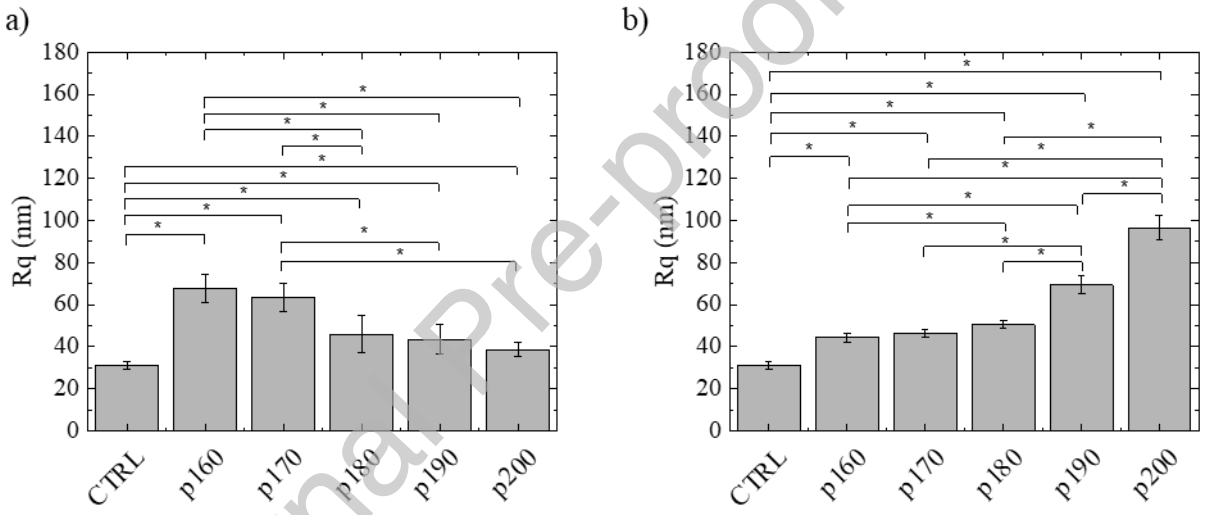

Figure 8*: Surface Roughness measurement (R_q) of bacteria cells on a) nanograting and b) nanopillars. Data were reported as mean value ± SD. Statistical significance is denoted by * p < 0.05.*

The alteration in *E. coli* morphology induced by the patterned substrates was further quantified by analyzing the high-resolution AFM topographies using ImageJ software. Specifically, each bacteria cell was automatically fitted with an ellipse using the fitting ellipse algorithm, and the axes were measured (Fig. 9 a and b). A significant decrease in the major axis of the bacteria on the p160 nanogratings was observed compared to the control, decreasing from (2.3 ± 0.2) μm to (1.8 ± 0.1) μm. In contrast, the minor axis length remained similar,

ranging from (1.0 ± 0.1) μm to (0.8 ± 0.1) μm. Additionally, as the nanogratings pitch increased, the major axis length also increased, from (1.7 ± 0.2) μm on p170 to (2.0 ± 0.2) μm on p200, while the minor axes remained relatively unchanged, varying from (0.8 ± 0.1) μm on p170 to (0.9 ± 0.1) μm on p200. Conversely, increasing the nanopillars pitch led to a decrease in the major axes of the *E. coli* cells, from (2.7 ± 0.2) μm on the control to (2.4± 0.4) μm on p160, and down to (1.3 ± 0.4) μm in p200 samples (Fig. 9b). Similarly to the cells grown on nanograting arrays, the nanopillars did not significantly modify the *E. coli* minor axes, ranging from (1.20 ± 0.02) μm in control to (1.0 ± 0.2) μm for the p200 nanopillar samples. The reduction in the major axes, coupled with the non-variation of the minor axes, clearly indicated that the bacteria bend along their main axis, assuming a curled shape. In conclusion, The most significant *E. coli* morphological changes were induced by nanopillars with higher pitches and nanogratings with lower pitches. Particularly, the reduction in the major axes, already observed in AFM and UHR SEM images (Fig.5, 6, and 7), confirms the transformation of the bacteria from a rod-shaped to a U-shaped morphology induced by the nanostructured surface.

Further analysis of the AFM images using NovaPx software quantified the changes in *E.coli* Surface Area (SA) and Volume induced by the nanopatterns (Fig. 9). The nanogratings with lower pitches caused a drastic reduction in the cellular surface area compared to control, decreasing from (2.8 ± 0.2) μm^2 to (1.4 ± 0.2) μm^2 of control and p160, respectively (Fig. 9a). With the increase in the nanogratings pitch, the cellular SA increased, reaching (1.8 ± 0.2) μm^2 for bacteria on p200 pillars. Conversely, the increase in the nanopillar's pitch induced an overall reduction in the *E. coli* SA, reaching the lowest value of (1.3 ± 0.2) μm^2 in the p200 sample (Fig. 9d).

Furthermore, the investigation of bacterial volume (Fig. 9f and e) revealed that the nanogratings induced a slight decrease in the *E. coli* volume, ranging from a 16% to 28%

reduction for nanograting with a larger pitch. A more pronounced variation in *E. coli* volume was observed in the p180, p190, and p200 nanopillar arrays, corresponding to a volume reduction of 32 %, 34%, and 40%, respectively.

It is well known that bacteria exhibit a multitude of shapes and each bacterial species has a proper and stable shape and dimensions. Additionally, within a bacterial population, cells typically show the same length and width, with a percentage of variation less than 4% [67]. Previous research has examined changes in microorganism cell morphology and dimensions in response to various stress conditions [68], including environmental stimuli [69], nutrient deprivation [70], antibiotic exposure [68] [71], and genetic modifications [72]. It is well established that severe alterations in bacterial morphology and volume are often related to stress, which directly leads to cell death.

The results obtained in our study demonstrated that, when bacteria interact with nanopatterned substrates, drastic changes in cell shape, surface area, and volume occur. These experimental findings, coupled with the observed increase in surface roughness, suggested that bacteria experienced significant stress upon contact with the nanostructured surface. Considering that both the nanopillar and nanograting arrays drastically reduced the number of bacteria on the surface and induced severe morphological changes, we concluded that these nanostructures constitute a hostile environment for the colonization and growth of the tested bacterial strain.

Similar results have been reported in previous studies investigating the antibacterial properties of nanostructured PMMA surfaces. For instance, M.N. Dickson and colleagues investigated the mechano-bactericidal activity of PMMA nanopillars with pitches of approximately 600 nm, 300 nm, and 200 nm realized by Nanoimprint lithography. In agreement with our data, their results showed that nanopillars with a periodicity of 200 nm

Journal Pre-proof

exhibited the highest antibacterial efficacy, highlighting the critical role of nanoscale feature dimensions in optimizing bactericidal performance [56]. S. Kim *et al*. realized nanopillars with a period of 300 nm on flat PMMA films by Nanoimprinting lithography and studied the attachment mechanism of both bacteria (*E*. *coli* and *P*. *aeruginosa*) and mammalian cells [73]. More recently, F. Viela and colleagues developed a PMMA-ZnO nanoparticle (NP) nanocomposite with nanopillars of about 250 nm spacing. The surface topography of the nanocomposite showed a broad-spectrum antibacterial activity, effectively inhibiting the growth of both Gram-positive bacteria, such as *Staphylococcus aureus*, and Gram-negative bacteria, including *E*. *coli* and *P*. *aeruginosa* [47]. While previous studies have demonstrated the antibacterial properties of PMMA nanostructured surfaces with different geometries, fabrication techniques, and composition (including the addition of antibacterial nanoparticles), the nanostructures described in our work have several significant advantages. The proposed nanofabrication approach using EBL provides a higher degree of precision and accuracy, enabling the creation of well-defined nanostructures with consistent feature dimensions in a single fabrication step. In addition, the EBL process used in our study is scalable, straightforward, and reproducible, providing a simpler and more reliable method for fabricating nanostructure compared to the nanoimprint and composite-based methods described in the aforementioned works. All these advantages lead us to believe that our nanostructures are very effective and versatile solutions for antibacterial applications.

Journal Pre-proof

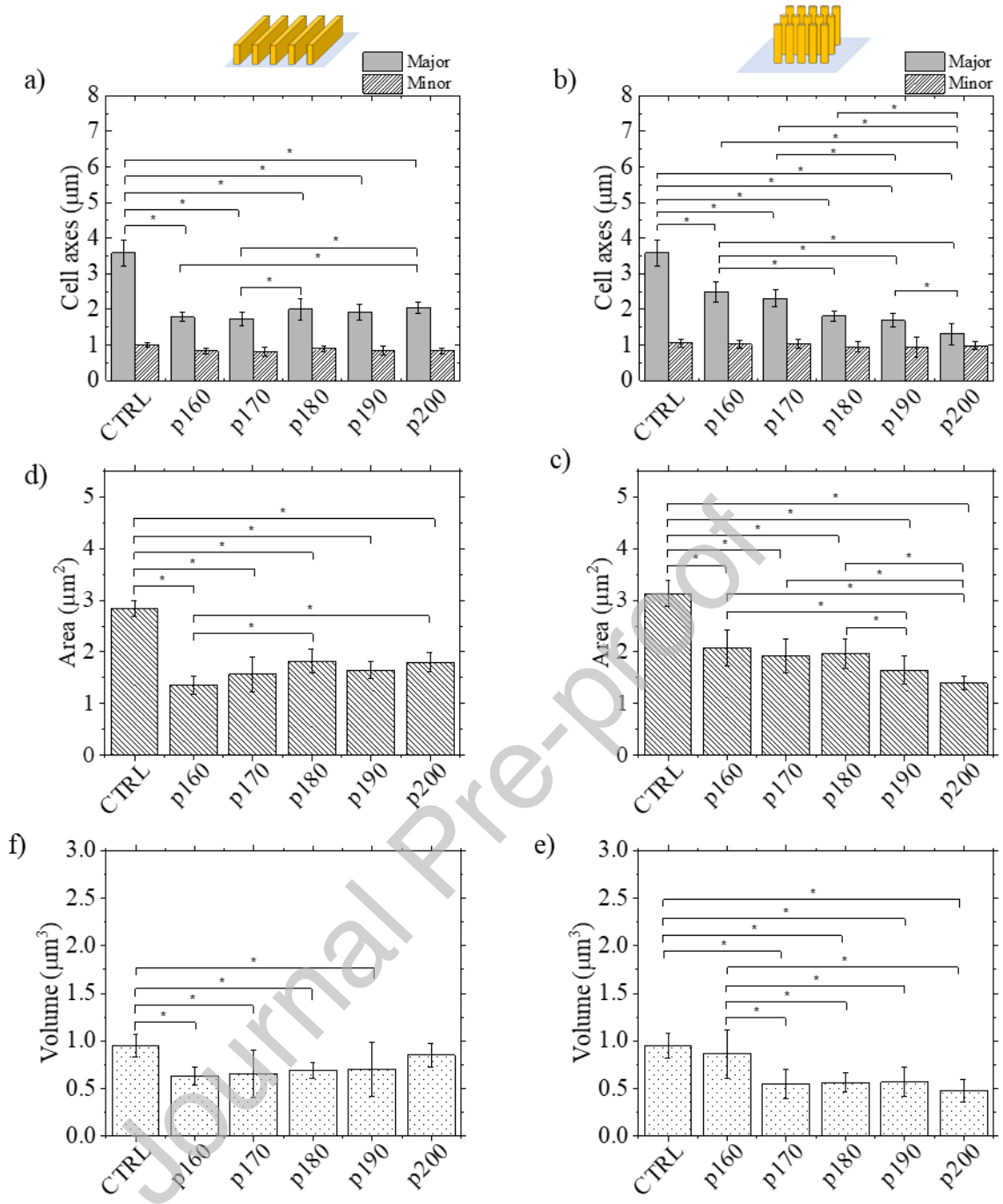

Journal Pre-proof

Figure 9. *Variation in cell morphology and dimension after interaction with the nanopatterned surface, measured on the high-resolution AFM topographies. Modification of the cell dimensions, in terms of a) and b) major and minor cell axes; c) and d) Surface Area, and f) and e) cell volumes of E. coli on nanogratings and nanopillars arrays, respectively. Data were reported as mean value ± SD. Statistical significance is denoted by * $p < 0.05$.*

Nanomechanical AFM Effect of nanostructures pitch on bactericidal properties.

A key indicator of cell health is elastic modulus [74], as it reflects the cell wall resistance to mechanical compression, as well as the stiffness of the peptidoglycan network and other cell wall components, such as surface biopolymers. *E. coli* grown on flat PMMA and arrays of nanogratings and nanopillars with varying pitches underwent nanomechanical characterization to quantify their elastic modulus, expressed as Young's modulus, and the Adhesion forces between AFM probe and bacteria surface. For this purpose, FD curves were randomly acquired on the bacterial surface and analyzed using Eq. (1) and (2), respectively (Fig. 9).

For *E. coli* cells grown on flat PMMA, Young's modulus was measured at (1.5 ± 0.2) MPa. This value significantly decreased to (0.7 ± 0.1) MPa for bacteria cultured on nanograting arrays with a pitch of 160 nm. As the nanograting pitch increased, the stiffness of *E. coli* progressively returned to that of the control value (Fig. 10 a). However, a different trend was observed for bacteria grown on nanopillar arrays, where increasing the distance between the pillars caused a notable reduction in Young's modulus. Specifically, the modulus decreases from (1.1 ± 0.1) MPa for the p160 to approximately (0.5 ± 0.1) MPa for p200 samples (Fig. 10 c).

Previous studies have investigated changes in bacterial elasticity in both antibiotic-susceptible and resistant cells using AFM force-indentation mode. These studies often report a reduction in cell elasticity and significant structural damage in susceptible cells following antibiotic exposure. This reduction in elasticity, coupled with evident structural damages, highlights the mechanical impact of antibiotics on bacterial cells and provides insight into their mechanisms of action and potential effectiveness [75] [76] [77] [78] [68]. It is well established that variations in bacterial stiffness are associated with ruptures or damage in the bacterial outer

Journal Pre-proof

membrane, followed by the degradation of the peptidoglycan layer, eventually leading to cell lysis [79]. The observed reduction in bacterial stiffness after contact with nanopatterned surfaces, along with the changes in the morphometrical parameters of *E. coli* cells described in the present study, suggests that the nanostructured surfaces exert sufficient stress to induce cell death.

Changes in the Adhesion forces between the silicon AFM tip and the bacterial surface can provide valuable insights into alterations in the chemical composition of the bacterial surface. By analyzing the retraction data of FD curves, it was determined that the adhesion force between the tip and the *E. coli* grown on the flat PMMA was (1.8 ± 0.1) nN. This value significantly increased to (18 ± 1.8) nN for bacteria on nanogratings with a pitch of 160 nm. In addition, with the increase of the nanogratings pitch, a corresponding decrease in the adhesion forces was observed, with the value dropping to (7.2 ± 0.1) nN for p170 and (4.3 ± 1.5) nN for p200 (Fig. 10 b). A similar trend was observed in the *E. coli* grown on the nanopillars array. However, in this case, the increase was more pronounced, resulting in equal to (14.8 ± 1.4) nN for the p160 and (16.7 ± 1.6) nN for p200 samples (Fig. 10 d).

The adhesion properties of bacterial cells are typically influenced by surface molecules such as lipopolysaccharides (LPS), peptidoglycans, and extruded biomacromolecules. Adhesion to surfaces is a complex and essential process for bacterial cells, supporting functions like nutrient acquisition, biofilm formation, and enhanced antibiotic resistance [68]. Previous AFM studies have demonstrated that bacterial adhesion forces increase in response to ampicillin, correlating with greater surface roughness in both susceptible *B. subtilis* and *E. coli* cells [68], [80]. Similarly, an increase in adhesion forces was observed in susceptible *P. aeruginosa* cells grown in biofilm cultures treated with nanoencapsulated colistin [81]. The increase in adhesion was attributed to the loss of internal cellular content following exposure to antibiotic and antimicrobial peptides. Therefore, the increment in adhesion forces between

the AFM tip and the cell's surface may result from the loss of biomolecules, changes in the expression of bacterial surface biomolecules, the loss of intracellular content, or the disruption of the outer bacterial membrane [81].

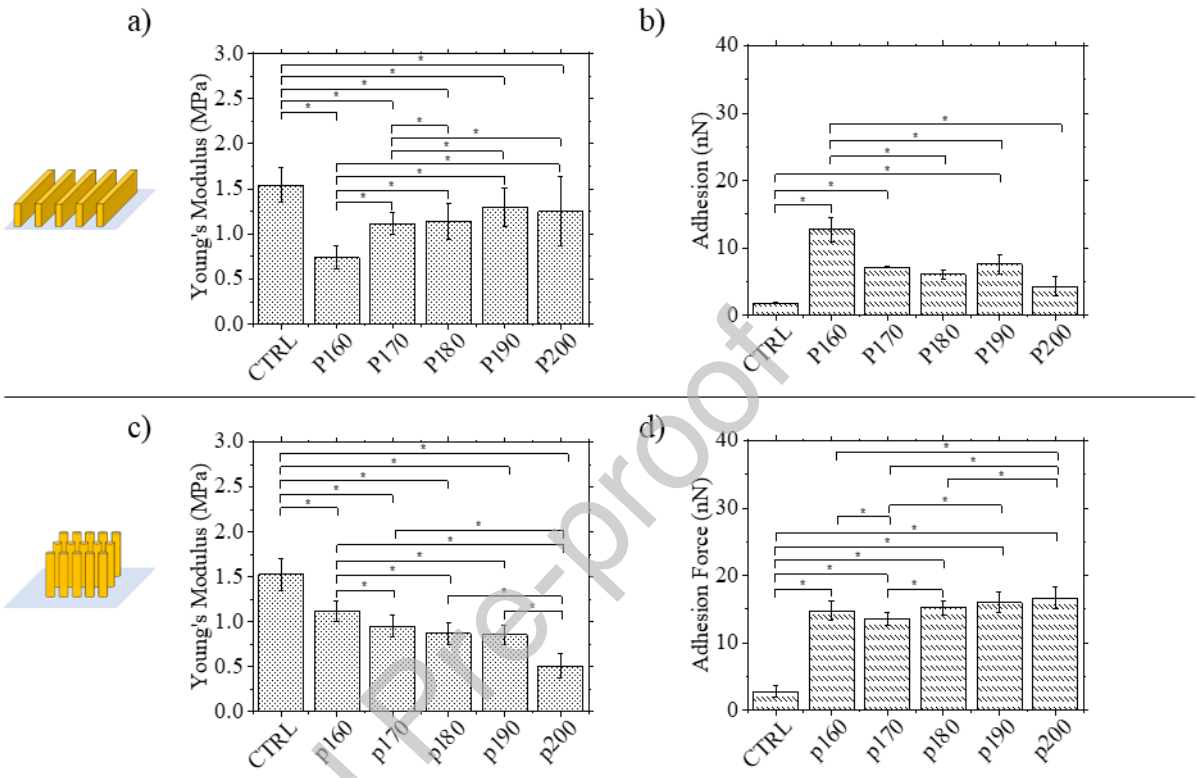

Figure 10. *Atomic Force Microscopy measurements of cell elasticity and adhesion forces between AFM tip and bacteria on a) and b) nangrating, c) and d) nanopillars. The data were reported as mean value ± SD. Statistical significance is denoted by * $p < 0.05$.*

Journal Pre-proof

The significant increase in adhesion forces observed in bacterial cells grown on both nanograting and nanopillar structures compared to the control suggests potential membrane damage or stress-induced alterations in the expression of surface molecules. This hypothesis is strongly supported by careful morphometric measurements detailed above, particularly the variation in surface rigidity induced by contact with the nanostructures and, above all, the increase in the surface roughness. These combined factors suggest that the nanostructured

surfaces may exert significant mechanical stress on the bacterial membranes, leading to changes in their chemical and physical properties.

CONCLUSION

Nanostructured surfaces have attracted significant scientific interest due to their ability to mechanically disrupt bacterial cells and reduce populations upon contact. However, the exact mechanisms underlying their bactericidal effects are not yet fully understood, highlighting the need for further investigation. To address this knowledge gap, we developed PMMA nanostructures using EBL, fabricating nanograting and nanopillar arrays with pitches ranging from 160 to 200 nm. These nanopatterned substrates were characterized using AFM and UHR SEM, and their antibacterial efficacy against *E. coli* was evaluated with the same technique. Our investigation revealed notable alterations in bacterial morphology, including changes in cell shape, size, and surface roughness. We observed a significant reduction in *E. coli* adhesion on nanopatterned surfaces, especially on nanopillars, and severe cell damage on both nanogratings and nanopillars. Additionally, the nanomechanical analysis showed decreased cell stiffness and increased adhesion forces between the AFM tip and bacteria surface, indicating that the nanostructured surfaces impose substantial stress on the microorganisms. This study offers valuable insights into the physical interactions between bacteria and nanostructured surfaces, providing a basis for future research aimed at improving the design and efficacy of antibacterial materials.

Journal Pre-proof

Declaration of generative AI and AI-assisted technologies in the writing process

During the preparation of this work, the authors used ChatGPT OpenAI to perform a grammar check of the manuscript. After using this tool, the authors reviewed and edited the content as needed and took full responsibility for the content of the published article.

CRediT authorship contribution statement

Paolo Pellegrino: Conceptualization, Data curation, Formal analysis, Investigation, Visualization, Writing – original draft, Writing – review and editing. **Isabella Farella**: Conceptualization, Investigation, Validation, Writing – original draft, Writing – review and editing. **Valeria De Matteis**: Conceptualization, Writing – review and editing. **Mariafrancesca Cascione**: Writing – review and editing. **Matteo Calcagnile**: Investigation, Writing – review and editing. **Stefania Villani**: Investigation, Writing – review and editing. **Lorenzo Vincenti**: Investigation, Writing – review and editing. **Pietro Alifano**: Writing – review and editing. **Fabio Quaranta**: Writing – review and editing. **Rosaria Rinaldi**: Supervision, Funding acquisition, Writing – review and editing.

Funding sources

This research received no specific grant from funding agencies in the public, commercial, or not-for-profit sectors.

Acknowledgments

The authors thank Mrs. Adriana Campa and Mr. Enrico Melissano for their strong and helpful technical support in the substrate preparation and Ti metal evaporation for the SEM analysis.

Journal Pre-proof

Reference

[1] F. Peyrusson *et al.*, «Intracellular Staphylococcus aureus persisters upon antibiotic exposure», *Nat. Commun.*, vol. 11, fasc. 1, p. 2200, mag. 2020, doi: 10.1038/s41467-020-15966-7.

[2] «Khardori et al. - 2020 - Antibiotics From the Beginning to the Future Par.pdf».

[3] N. Khardori, C. Stevaux, e K. Ripley, «Antibiotics: From the Beginning to the Future: Part 1», *Indian J. Pediatr.*, vol. 87, fasc. 1, pp. 39–42, gen. 2020, doi: 10.1007/s12098-019-03087-z.

[4] K. E. Jones *et al.*, «Global trends in emerging infectious diseases», *Nature*, vol. 451, fasc. 7181, pp. 990–993, feb. 2008, doi: 10.1038/nature06536.

[5] «A shot in the arm.pdf».

[6] F. Akram, M. Imtiaz, e I. U. Haq, «Emergent crisis of antibiotic resistance: A silent pandemic threat to 21st century», *Microb. Pathog.*, vol. 174, p. 105923, gen. 2023, doi: 10.1016/j.micpath.2022.105923.

[7] Satoru Kimura, Yasuhide Nakamura, *Poor Quality Pharmaceuticals in Global Public Health*. in Trust. Springer Singapore. [Online]. Disponibile su: https://doi.org/10.1007/978-981-15-2089-1

[8] P. N. Newton, M. D. Green, e F. M. Fernández, «Impact of poor-quality medicines in the 'developing' world», *Trends Pharmacol. Sci.*, vol. 31, fasc. 3, pp. 99–101, mar. 2010, doi: 10.1016/j.tips.2009.11.005.

[9] A. Tripathy, P. Sen, B. Su, e W. H. Briscoe, «Natural and bioinspired nanostructured bactericidal surfaces», *Adv. Colloid Interface Sci.*, vol. 248, pp. 85–104, ott. 2017, doi: 10.1016/j.cis.2017.07.030.

[10] N. R. Naylor *et al.*, «Estimating the burden of antimicrobial resistance: a systematic literature review», *Antimicrob. Resist. Infect. Control*, vol. 7, fasc. 1, p. 58, apr. 2018, doi: 10.1186/s13756-018-0336-y.

[11] «Current Treatment Strategies Against Multidrug-Resistant Bacteria A Review.pdf».

[12] H. Haidari *et al.*, «Polycationic Silver Nanoclusters Comprising Nanoreservoirs of Ag^+ Ions with High Antimicrobial and Antibiofilm Activity», *ACS Appl. Mater. Interfaces*, vol. 14, fasc. 1, pp. 390–403, gen. 2022, doi: 10.1021/acsami.1c21657.

[13] L. Wang, W. Zheng, S. Li, L. Zhong, e X. Jiang, «Aminophenol-Decorated Gold Nanoparticles for Curing Bacterial Infections», *Nano Lett.*, vol. 22, fasc. 9, pp. 3576–3582, mag. 2022, doi: 10.1021/acs.nanolett.1c04968.

[14] N. G. Durmus, E. N. Taylor, K. M. Kummer, e T. J. Webster, «Enhanced Efficacy of Superparamagnetic Iron Oxide Nanoparticles Against Antibiotic-Resistant Biofilms in the Presence of Metabolites», *Adv. Mater.*, vol. 25, fasc. 40, pp. 5706–5713, ott. 2013, doi: 10.1002/adma.201302627.

[15] A. Díez-Pascual, «Antibacterial Activity of Nanomaterials», *Nanomaterials*, vol. 8, fasc. 6, p. 359, mag. 2018, doi: 10.3390/nano8060359.

[16] P. Kumar, P. Huo, R. Zhang, e B. Liu, «Antibacterial Properties of Graphene-Based Nanomaterials», *Nanomaterials*, vol. 9, fasc. 5, p. 737, mag. 2019, doi: 10.3390/nano9050737.

[17] M. Azizi-Lalabadi, H. Hashemi, J. Feng, e S. M. Jafari, «Carbon nanomaterials against pathogens; the antimicrobial activity of carbon nanotubes, graphene/graphene oxide, fullerenes, and their nanocomposites», *Adv. Colloid Interface Sci.*, vol. 284, p. 102250, ott. 2020, doi: 10.1016/j.cis.2020.102250.

[18] A. Kassem, G. M. Ayoub, e L. Malaeb, «Antibacterial activity of chitosan nano-composites and carbon nanotubes: A review», *Sci. Total Environ.*, vol. 668, pp. 566–576, giu. 2019, doi: 10.1016/j.scitotenv.2019.02.446.

[19] H. M. H. N. Bandara, M. J. Herpin, D. Kolacny, A. Harb, D. Romanovicz, e H. D. C. Smyth, «Incorporation of Farnesol Significantly Increases the Efficacy of Liposomal Ciprofloxacin against *Pseudomonas aeruginosa* Biofilms *in Vitro*», *Mol. Pharm.*, vol. 13, fasc. 8, pp. 2760–2770, ago. 2016, doi: 10.1021/acs.molpharmaceut.6b00360.

Journal Pre-proof

[20] M.-K. Yeh, Hsin-I Chang, e Ming-Yen Cheng, «Clinical development of liposome based drugs: formulation, characterization, and therapeutic efficacy», *Int. J. Nanomedicine*, p. 49, dic. 2011, doi: 10.2147/IJN.S26766.
[21] C. Ergene, K. Yasuhara, e E. F. Palermo, «Biomimetic antimicrobial polymers: recent advances in molecular design», *Polym. Chem.*, vol. 9, fasc. 18, pp. 2407–2427, 2018, doi: 10.1039/C8PY00012C.
[22] S. D. Ganesh, N. Saha, O. Zandraa, R. N. Zuckermann, e P. Sáha, «Peptoids and polypeptoids: biomimetic and bioinspired materials for biomedical applications», *Polym. Bull.*, vol. 74, fasc. 8, pp. 3455–3466, ago. 2017, doi: 10.1007/s00289-016-1902-1.
[23] S. Villani *et al.*, «Neem-hypericum-bacterial cellulose wound care paste characterized in vitro and in Galleria mellonella in vivo model», *Carbohydr. Polym. Technol. Appl.*, vol. 7, p. 100431, giu. 2024, doi: 10.1016/j.carpta.2024.100431.
[24] «Physica Status Solidi a - 2022 - Velardi - Correlation between Photocatalysis and Antibacterial Responses of Cu-Doped TiO2.pdf».
[25] «Nanomaterial-based therapeutics for antibiotic-resistant bacterial infections.pdf».
[26] W. Chen *et al.*, «Bacterial acidity-triggered antimicrobial activity of self-assembling peptide nanofibers», *J. Mater. Chem. B*, vol. 7, fasc. 18, pp. 2915–2919, 2019, doi: 10.1039/C9TB00134D.
[27] C. Qu *et al.*, «Bio-inspired antimicrobial surfaces fabricated by glancing angle deposition», *Sci. Rep.*, vol. 13, fasc. 1, p. 207, gen. 2023, doi: 10.1038/s41598-022-27225-4.
[28] J. Hasan *et al.*, «Selective bactericidal activity of nanopatterned superhydrophobic cicada Psaltoda claripennis wing surfaces», *Appl. Microbiol. Biotechnol.*, vol. 97, fasc. 20, pp. 9257–9262, ott. 2013, doi: 10.1007/s00253-012-4628-5.
[29] S. M. Kelleher *et al.*, «Cicada Wing Surface Topography: An Investigation into the Bactericidal Properties of Nanostructural Features», *ACS Appl. Mater. Interfaces*, vol. 8, fasc. 24, pp. 14966–14974, giu. 2016, doi: 10.1021/acsami.5b08309.
[30] S. H. T. Nguyen, H. K. Webb, J. Hasan, M. J. Tobin, R. J. Crawford, e E. P. Ivanova, «Dual role of outer epicuticular lipids in determining the wettability of dragonfly wings», *Colloids Surf. B Biointerfaces*, vol. 106, pp. 126–134, giu. 2013, doi: 10.1016/j.colsurfb.2013.01.042.
[31] «Investigation on large-area fabrication of vivid shark skin with.pdf».
[32] «A new method for producing ‘‘Lotus Effect’’ on a biomimetic shark skin.pdf».
[33] D. L. Gonzalez Arellano *et al.*, «Gecko-Inspired Biocidal Organic Nanocrystals Initiated from a Pencil-Drawn Graphite Template», *Sci. Rep.*, vol. 8, fasc. 1, p. 11618, ago. 2018, doi: 10.1038/s41598-018-29994-3.
[34] G. S. Watson *et al.*, «A gecko skin micro/nano structure – A low adhesion, superhydrophobic, anti-wetting, self-cleaning, biocompatible, antibacterial surface», *Acta Biomater.*, vol. 21, pp. 109–122, lug. 2015, doi: 10.1016/j.actbio.2015.03.007.
[35] D. Chopra, K. Gulati, e S. Ivanovski, «Bed of nails: bioinspired nano-texturing towards antibacterial and bioactivity functions», *Mater. Today Adv.*, vol. 12, p. 100176, dic. 2021, doi: 10.1016/j.mtadv.2021.100176.
[36] N. Lin, P. Berton, C. Moraes, R. D. Rogers, e N. Tufenkji, «Nanodarts, nanoblades, and nanospikes: Mechano-bactericidal nanostructures and where to find them», *Adv. Colloid Interface Sci.*, vol. 252, pp. 55–68, feb. 2018, doi: 10.1016/j.cis.2017.12.007.
[37] E. P. Ivanova *et al.*, «Natural Bactericidal Surfaces: Mechanical Rupture of *Pseudomonas aeruginosa* Cells by Cicada Wings», *Small*, vol. 8, fasc. 16, pp. 2489–2494, ago. 2012, doi: 10.1002/smll.201200528.
[38] E. P. Ivanova *et al.*, «Bactericidal activity of black silicon», *Nat. Commun.*, vol. 4, fasc. 1, p. 2838, nov. 2013, doi: 10.1038/ncomms3838.
[39] C. D. Bandara *et al.*, «Bactericidal Effects of Natural Nanotopography of Dragonfly Wing on *Escherichia coli*», *ACS Appl. Mater. Interfaces*, vol. 9, fasc. 8, pp. 6746–6760, mar. 2017, doi: 10.1021/acsami.6b13666.

Journal Pre-proof

[40] D. P. Linklater *et al.*, «Nanopillar Polymer Films as Antibacterial Packaging Materials», *ACS Appl. Nano Mater.*, vol. 5, fasc. 2, pp. 2578–2591, feb. 2022, doi: 10.1021/acsanm.1c04251.
[41] S. Wu, F. Zuber, K. Maniura-Weber, J. Brugger, e Q. Ren, «Nanostructured surface topographies have an effect on bactericidal activity», *J. Nanobiotechnology*, vol. 16, fasc. 1, p. 20, dic. 2018, doi: 10.1186/s12951-018-0347-0.
[42] J. Jenkins *et al.*, «Antibacterial effects of nanopillar surfaces are mediated by cell impedance, penetration and induction of oxidative stress», *Nat. Commun.*, vol. 11, fasc. 1, p. 1626, apr. 2020, doi: 10.1038/s41467-020-15471-x.
[43] S. Han, S. Ji, A. Abdullah, D. Kim, H. Lim, e D. Lee, «Superhydrophilic nanopillar-structured quartz surfaces for the prevention of biofilm formation in optical devices», *Appl. Surf. Sci.*, vol. 429, pp. 244–252, gen. 2018, doi: 10.1016/j.apsusc.2017.07.164.
[44] A. Valiei *et al.*, «Hydrophilic Mechano-Bactericidal Nanopillars Require External Forces to Rapidly Kill Bacteria», *Nano Lett.*, vol. 20, fasc. 8, pp. 5720–5727, ago. 2020, doi: 10.1021/acs.nanolett.0c01343.
[45] L. E. Fisher, Y. Yang, M.-F. Yuen, W. Zhang, A. H. Nobbs, e B. Su, «Bactericidal activity of biomimetic diamond nanocone surfaces», *Biointerphases*, vol. 11, fasc. 1, p. 011014, mar. 2016, doi: 10.1116/1.4944062.
[46] T. Diu *et al.*, «Cicada-inspired cell-instructive nanopatterned arrays», *Sci. Rep.*, vol. 4, fasc. 1, p. 7122, nov. 2014, doi: 10.1038/srep07122.
[47] F. Viela *et al.*, «Nano-engineering safer-by-design nanoparticle based moth-eye mimetic bactericidal and cytocompatible polymer surfaces», *RSC Adv.*, vol. 8, fasc. 40, pp. 22606–22616, 2018, doi: 10.1039/C8RA03403F.
[48] M. Hirano, M. Hashimoto, K. Miura, e N. Ohtsu, «Fabrication of antibacterial nanopillar surface on AISI 316 stainless steel through argon plasma etching with direct current discharge», *Surf. Coat. Technol.*, vol. 406, p. 126680, gen. 2021, doi: 10.1016/j.surfcoat.2020.126680.
[49] Y. Tang, H. Sun, Z. Qin, S. Yin, L. Tian, e Z. Liu, «Bioinspired photocatalytic ZnO/Au nanopillar-modified surface for enhanced antibacterial and antiadhesive property», *Chem. Eng. J.*, vol. 398, p. 125575, ott. 2020, doi: 10.1016/j.cej.2020.125575.
[50] S. Hawi, S. Goel, V. Kumar, O. Pearce, W. N. Ayre, e E. P. Ivanova, «Critical Review of Nanopillar-Based Mechanobactericidal Systems», *ACS Appl. Nano Mater.*, vol. 5, fasc. 1, pp. 1–17, gen. 2022, doi: 10.1021/acsanm.1c03045.
[51] E. P. Ivanova *et al.*, «The multi-faceted mechano-bactericidal mechanism of nanostructured surfaces», *Proc. Natl. Acad. Sci. U. S. A.*, vol. 117, fasc. 23, pp. 12598–12605, 2020, doi: 10.1073/pnas.1916680117.
[52] C. Zhu, H. Ekinci, A. Pan, B. Cui, e X. Zhu, «Electron beam lithography on nonplanar and irregular surfaces», *Microsyst. Nanoeng.*, vol. 10, fasc. 1, p. 52, apr. 2024, doi: 10.1038/s41378-024-00682-9.
[53] S. N. Khonina, N. L. Kazanskiy, e M. A. Butt, «Grayscale Lithography and a Brief Introduction to Other Widely Used Lithographic Methods: A State-of-the-Art Review», *Micromachines*, vol. 15, fasc. 11, p. 1321, ott. 2024, doi: 10.3390/mi15111321.
[54] R. Mudachathi e T. Tanaka, «Up Scalable Full Colour Plasmonic Pixels with Controllable Hue, Brightness and Saturation», *Sci. Rep.*, vol. 7, fasc. 1, p. 1199, apr. 2017, doi: 10.1038/s41598-017-01266-6.
[55] X. Wang, J. Xu, X. Quan, Y. Li, Y. Wang, e X. Cheng, «Fast fabrication of silicon nanopillar array using electron beam lithography with two-layer exposure method», *Microelectron. Eng.*, vol. 227, p. 111311, apr. 2020, doi: 10.1016/j.mee.2020.111311.
[56] M. N. Dickson, E. I. Liang, L. A. Rodriguez, N. Vollereaux, e A. F. Yee, «Nanopatterned polymer surfaces with bactericidal properties», *Biointerphases*, vol. 10, fasc. 2, p. 021010, 2015, doi: 10.1116/1.4922157.

Journal Pre-proof

[57] E. P. Goldschmidt, M. S. Cater, T. S. Matney, M. Ann Butler, e A. Greene, «GENETIC ANALYSIS OF THE HISTIDINE OPERON IN *ESCHERICHIA COLI* K12», *Genetics*, vol. 66, fasc. 2, pp. 219–229, ott. 1970, doi: 10.1093/genetics/66.2.219.
[58] D. Vinella e R. D'Ari, «Thermoinducible filamentation in Escherichia coli due to an altered RNA polymerase beta subunit is suppressed by high levels of ppGpp», *J. Bacteriol.*, vol. 176, fasc. 4, pp. 966–972, feb. 1994, doi: 10.1128/jb.176.4.966-972.1994.
[59] «Talà et al. - 2022 - Phenotyping of Fecal Microbiota of Winnie, a Roden.pdf».
[60] S. Belikov, J. Alexander, C. Wall, I. Yermolenko, S. Magonov, e I. Malovichko, «Thermal tune method for AFM oscillatory resonant imaging in air and liquid», in *2014 American Control Conference*, Portland, OR, USA: IEEE, giu. 2014, pp. 1009–1014. doi: 10.1109/ACC.2014.6859224.
[61] K. Modaresifar *et al.*, «Deciphering the Roles of Interspace and Controlled Disorder in the Bactericidal Properties of Nanopatterns against Staphylococcus aureus», *Nanomaterials*, vol. 10, fasc. 2, p. 347, feb. 2020, doi: 10.3390/nano10020347.
[62] M. Ganjian *et al.*, «Nature Helps: Toward Bioinspired Bactericidal Nanopatterns», *Adv. Mater. Interfaces*, vol. 6, fasc. 16, 2019, doi: 10.1002/admi.201900640.
[63] C. D. Bandara *et al.*, «Bactericidal Effects of Natural Nanotopography of Dragonfly Wing on Escherichia coli», *ACS Appl. Mater. Interfaces*, vol. 9, fasc. 8, pp. 6746–6760, 2017, doi: 10.1021/acsami.6b13666.
[64] Y. Liu, J. Strauss, e T. A. Camesano, «Adhesion forces between Staphylococcus epidermidis and surfaces bearing self-assembled monolayers in the presence of model proteins», *Biomaterials*, vol. 29, fasc. 33, pp. 4374–4382, nov. 2008, doi: 10.1016/j.biomaterials.2008.07.044.
[65] M. Michalska *et al.*, «Tuning antimicrobial properties of biomimetic nanopatterned surfaces», *Nanoscale*, vol. 10, fasc. 14, pp. 6639–6650, 2018, doi: 10.1039/c8nr00439k.
[66] D. P. Linklater, V. A. Baulin, S. Juodkazis, R. J. Crawford, P. Stoodley, e E. P. Ivanova, «Mechano-bactericidal actions of nanostructured surfaces», *Nat. Rev. Microbiol.*, vol. 19, fasc. 1, pp. 8–22, gen. 2021, doi: 10.1038/s41579-020-0414-z.
[67] K. D. Young, «Bacterial Shape: Two-Dimensional Questions and Possibilities», *Annu. Rev. Microbiol.*, vol. 64, fasc. 1, pp. 223–240, ott. 2010, doi: 10.1146/annurev.micro.112408.134102.
[68] S. C. Uzoechi e N. I. Abu-Lail, «Variations in the Morphology, Mechanics and Adhesion of Persister and Resister E. coli Cells in Response to Ampicillin: AFM Study», *Antibiotics*, vol. 9, fasc. 5, p. 235, mag. 2020, doi: 10.3390/antibiotics9050235.
[69] H. Shi *et al.*, «Precise regulation of the relative rates of surface area and volume synthesis in bacterial cells growing in dynamic environments», *Nat. Commun.*, vol. 12, fasc. 1, p. 1975, mar. 2021, doi: 10.1038/s41467-021-22092-5.
[70] A. Typas, M. Banzhaf, C. A. Gross, e W. Vollmer, «From the regulation of peptidoglycan synthesis to bacterial growth and morphology», *Nat. Rev. Microbiol.*, vol. 10, fasc. 2, pp. 123–136, feb. 2012, doi: 10.1038/nrmicro2677.
[71] H.-N. Su *et al.*, «Antimicrobial Peptide Trichokonin VI-Induced Alterations in the Morphological and Nanomechanical Properties of Bacillus subtilis», *PLoS ONE*, vol. 7, fasc. 9, p. e45818, set. 2012, doi: 10.1371/journal.pone.0045818.
[72] H. Vashistha, J. Jammal-Touma, K. Singh, Y. Rabin, e H. Salman, «Bacterial cell-size changes resulting from altering the relative expression of Min proteins», *Nat. Commun.*, vol. 14, fasc. 1, p. 5710, set. 2023, doi: 10.1038/s41467-023-41487-0.
[73] S. Kim *et al.*, «Nanostructured Multifunctional Surface with Antireflective and Antimicrobial Characteristics», *ACS Appl. Mater. Interfaces*, vol. 7, fasc. 1, pp. 326–331, gen. 2015, doi: 10.1021/am506254r.
[74] A. Zdarta e E. Kaczorek, «Nanomechanical changes in probiotic bacteria under antibiotics exposure: Implications on Lactobacillus biofilm formation», *Biochim. Biophys. Acta BBA - Mol. Cell Res.*, vol. 1870, fasc. 7, p. 119533, ott. 2023, doi: 10.1016/j.bbamcr.2023.119533.

Journal Pre-proof

[75] G. Longo *et al.*, «Rapid detection of bacterial resistance to antibiotics using AFM cantilevers as nanomechanical sensors», *Nat. Nanotechnol.*, vol. 8, fasc. 7, pp. 522–526, lug. 2013, doi: 10.1038/nnano.2013.120.
[76] S. C. Uzoechi e N. I. Abu-Lail, «Changes in cellular elasticities and conformational properties of bacterial surface biopolymers of multidrug-resistant Escherichia coli (MDR-E. coli) strains in response to ampicillin», *Cell Surf.*, vol. 5, p. 100019, dic. 2019, doi: 10.1016/j.tcsw.2019.100019.
[77] «Atomic force microscopy study of theantimicrobial activity of aqueous garlic versusampicillin against Escherichia coli andStaphylococcus aureu.pdf».
[78] P. C. Braga e D. Ricci, «Atomic Force Microscopy: Application to Investigation of *Escherichia coli* Morphology before and after Exposure to Cefodizime», *Antimicrob. Agents Chemother.*, vol. 42, fasc. 1, pp. 18–22, gen. 1998, doi: 10.1128/AAC.42.1.18.
[79] M. Cieśluk *et al.*, «Physics Comes to the Aid of Medicine—Clinically-Relevant Microorganisms through the Eyes of Atomic Force Microscope», *Pathogens*, vol. 9, fasc. 11, p. 969, nov. 2020, doi: 10.3390/pathogens9110969.
[80] D. Laskowski, J. Strzelecki, K. Pawlak, H. Dahm, e A. Balter, «Effect of ampicillin on adhesive properties of bacteria examined by atomic force microscopy», *Micron*, vol. 112, pp. 84–90, set. 2018, doi: 10.1016/j.micron.2018.05.005.
[81] E. Sans-Serramitjana *et al.*, «Killing effect of nanoencapsulated colistin sulfate on Pseudomonas aeruginosa from cystic fibrosis patients», *J. Cyst. Fibros.*, vol. 15, fasc. 5, pp. 611–618, set. 2016, doi: 10.1016/j.jcf.2015.12.005.

Author Statement

We the undersigned declare that this manuscript is original, has not been published before and is not currently being considered for publication elsewhere.

We confirm that the manuscript has been read and approved by all named authors and that there are no other persons who satisfied the criteria for authorship but are not listed. We further confirm that the order of authors listed in the manuscript has been approved by all of us.

We understand that the Corresponding Author is the sole contact for the Editorial process. He/she is responsible for communicating with the other authors about progress, submissions of revisions and final approval of proofs

Journal Pre-proof

Graphical Abstract

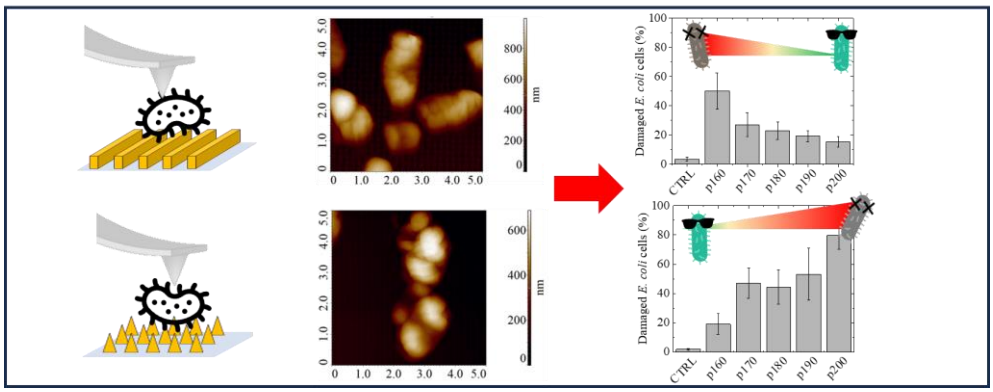

Declaration of interests

☒ The authors declare that they have no known competing financial interests or personal relationships that could have appeared to influence the work reported in this paper.

☐ The authors declare the following financial interests/personal relationships which may be considered as potential competing interests:

Journal Pre-proof